A PULSE NMR TRILOGY:
ANOMALIES, ANISOTROPIES, AND ADSORPTION

Thesis by

Loren Bennett Schreiber

In Partial Fulfillment of the Requirements

for the Degree of

Doctor of Philosophy

California Institute of Technology

Pasadena, California

1975

(Submitted May 28, 1975)

To my parents

It is a tree of life to them that hold fast to it,

and its supporters are happy.

Its ways are ways of pleasantness,

and all its paths are peace.

-Proverbs 3:18, 17

ACKNOWLEDGEMENTS

I came to Cal Tech to learn. To learn about science, about people, and about myself. With the help of teachers, facilities, time, and freedom, I learned about these things.

Professor Robert W. Vaughan willingly gave much time and effort as my research advisor. In fact, I did not even have to ask for his exceptionally detailed guidance on the many technical problems which arose nor for his extensive assistance with the examination and interpretation of my data. He also patiently counseled me throughout my years here. However, most importantly, Vaughan taught me how to do an experiment. I hope that my efforts as reported in this thesis adequately reflect the efforts he has given so generously and I hope that he is pleased and maybe even proud of the scientific development of his first graduate student.

Since my arrival at Cal Tech was in the middle of the academic year, it was impossible at that point for me to take any courses. As a result, I had to encounter immediately the initial barrier of getting started in the laboratory. I am grateful for the technical instruction, the emotional support, and the gentle push of Larry Stacey and Ed Olli to help me to surmount this barrier and plunge right into research.

Getting the laboratory started on campus was not so simple and was possible only because of the expert craftmanship and sound advice of Ray Reed and George Griffith. The many suggestions of Hollis Reamer were also helpful as was the equipment which was all so well built by Chic Nakawatase, Bill Schuelke, and Henry Smith.

John Yehle did an outstanding job both at building the spectrometer and also teaching me some of the principles and strategy of electronics. His hard work, advice, and encouragement during numerous breakdowns is deeply appreciated. Without question he is the most valuable member of our research group.

My initial start at learning NMR theory was also difficult for me. I thank Sunney Chan who, rather than embarrassing me, instead encouraged me to ask many questions, though usually stupid, during his

NMR course. The numerous discussions both on NMR and personal matters with Dan Elleman and Won-Kyu Rhim were always illuminating and enjoyable.

I was indeed fortunate that Henry Weinberg came to this campus since he advised me often and well on my surface research and overall research program. In many ways, he was a second research advisor to me. His understanding and sympathy, particularly when it was lacking from others, will always be remembered.

I also had the opportunity to learn some physics from three close friends in the research group, Larry Stacey, Kei-Fung Lau, and Mike Stoll. Unfortunately, in our frequent discussions, I was rarely able to come up with good answers. I hope that at least I was able to ask some good questions.

Most of all, I am grateful for my friendships with Glenn Laguna, Grant Robertson, and Erdinc Zana with whom I shared the joys and frustrations of graduate school.

Many organizations also provided substantial contributions not the least of which were the Union Oil Company and the National Science Foundation.

Tantalizing and sumptuous meals at a number of fine restaurants in the area provided much enjoyment and relaxation. The following were consistently good: The Konditori, Ernie Jr's, The Acapulco, Dino's, and especially, The Souvlaki.

Real inspiration was instilled by the many great films shown in the area. Television Channels 5, 9, 11, and 28 and the local theaters, the Esquire, Academy, State, Uptown, Colorado, and Pasadena UA, have all done a good job. On campus, Cinematech and the Silent Film Festivals at Beckman have been outstanding. I also wish to thank Channel 9 for re-running Have Gun Will Travel and The Avengers and Channel 5 for re-running The Prisoner.

Finally I would like to thank the California Institute of Technology which gave me much time and freedom to learn, to think, and to travel on stupendous trips to Rio de Janeiro and to East Africa.

ABSTRACT

In phase one of this thesis, a systematic method, an extension of the average Hamiltonian formalism, is presented for calculating the effects of pulse errors in the multiple pulse nuclear magnetic resonance (NMR) experiments. Application of this method to account for effects of pulse nonidealities such as phase errors, phase transient effects, pulse size errors, and rf inhomogeneity is found to agree with experimental observation.

In phase two, the proton chemical shift tensor of the hydroxyl proton in calcium hydroxide was measured using multiple pulse NMR techniques. The tensor is axially symmetric with susceptibility corrected components of $\sigma_{\perp} = -9.3 \pm 1$ ppm and $\sigma_{\parallel} = +4.7 \pm 1$ ppm relative to TMS.

In phase three, conventional and multiple pulse NMR techniques were used to examine the hydroxyl protons on a series of high surface area silica-aluminas whose composition varied from 0-100% SiO_2. Protons remaining on these materials after being calcined at 500°C are found to exist as immobile and isolated hydroxyl groups at room temperature. With the high silica content samples, 100-75% SiO_2, no AlOH groups were detectable, while on the 50% and lower SiO_2 content samples, most protons were in AlOH groups; thus, there is indication of a major change in local structure between 75% and 50% silica content.

TABLE OF CONTENTS

CHAPTER 1

INTRODUCTION

THE FOUR QUESTIONS

At first glance, the three investigations which are presented in the following chapters may appear to be unconnected. It is the purpose of this introduction to show that these three studies are in fact united. They are united by the common goal of developing multiple pulse nuclear magnetic resonance (NMR) into a practical spectroscopic technique capable of routinely furnishing valuable information about physical and chemical phenomena.

Unfortunately this goal was not reached by this thesis research. But steps were taken in the right direction; a finite amount of forward progress was made. The theoretical understanding of the effects of pulse imperfections has been sufficiently improved so that theory has pointed the way to eliminating these effects experimentally in a rational manner. Improvements in equipment design (and also a lot of money from research grants) have enabled multiple pulse NMR experiments to be conducted successfully under substantially adverse conditions such as poor signal-to-noise and strong dipolar couplings. Finally, the physical insight into multiple pulse NMR has matured so that these techniques have been used to help sort out the many possible interactions present in a complicated adsorption system.

In order to orient further the reader, yet to prevent idle rambling, the discussion in the remainder of this chapter will center upon answering the following four questions:

(1) Other NMR experiments, although simple technically, produce spectra that are often difficult to interpret. Why do multiple pulse experiments, although complicated technically, often

simplify the interpretation of NMR spectra?

(2) All other calculations of the anomalies that are caused by pulse imperfections and observed in multiple pulse NMR spectra are awkward, limited, and often incorrect. Why is the method presented in this thesis for calculating effects of pulse errors simple, systematic, and straightforward?

(3) Conventional NMR experiments yield at most the isotropic portion of the proton chemical shift tensor. How does multiple pulse NMR furnish all three principal values of the chemical shift tensor and, in particular, why is this anisotropic information for $Ca(OH)_2$ useful?

(4) Previous NMR investigations of gas-solid adsorption systems have been hampered by numerous theoretical and experimental obstacles. How were these difficulties overcome in the study presented in this thesis?

ANSWER TO QUESTION 1

Let's first briefly review conventional cw NMR experiments (1,2). The total Hamiltonian is the sum of Hamiltonians for the lattice, for the coupling of the nuclear spins to the applied magnetic field (nuclear Zeeman effect), for the coupling of the nuclear spins to the lattice, and for the coupling of the nuclear spins with the rf field.

$$H = H_o^{L} + H_o^{S} + H_i^{SL} + H_{rf} \qquad (1)$$

The lattice is defined here as the entire system under consideration but with all nuclei having zero spin. A major goal of applied

spectroscopy is to improve our knowledge, which is at present only crude, of the stationary states of the lattice Hamiltonian. To accomplish this, experimentalists have adopted the following strategy which can be divided into three parts. Part 1, measure parameters obtained by the perturbation of the lattice on the observable states. Part 2, relate these parameters to the expectation values of the perturbation operator. Part 3, correlate these parameters with models of the lattice. Thus, although the lattice wave function cannot be measured, the parameters or expectation values which can be measured may indirectly provide substantial information about the structure of the lattice wave function.

The goal of NMR experiments is usually to learn about the lattice through its perturbation on the spin states. The perturbing interaction is the spin-lattice coupling, H_i^{SL}. Examples of spin-lattice couplings include the nuclear dipolar interaction, nuclear quadrupolar coupling, chemical shift coupling, spin-spin coupling, Knight shift, and hyperfine coupling. Each spin-lattice Hamiltonian is a product of a spin operator, which operates on lattice wave functions. Each spin-lattice Hamiltonian may be alternatively represented as a product of a spin operator and a spin-lattice parameter. A major emphasis of standard textbooks (1,2) is to relate, for a given spin-lattice Hamiltonian, the spin-lattice parameter to matrix elements of the corresponding lattice operator (that is, part 2 of the above experimental strategy).

Although the spin-lattice parameters provide useful information because they perturb the lattice, these parameters are most easily measured by detecting their effects upon the spin system. Typically, the magnitudes of the applied magnetic field, H_0, and of the rf field,

H_1, are adjusted to satisfy the conditions

$$H_o^L >> H_o^S >> H_i^{SL} >> H_{rf} \tag{2}$$

where H_o^S has the form

$$H_o^S = - \gamma\hbar H_o I_z \tag{3}$$

and H_{rf} has the following simple form in the rotating frame

$$H_{rf} = - \gamma\hbar H_o I_x. \tag{4}$$

In Equations 3 and 4, γ is the gyromagnetic ratio of the nucleus, and I_x and I_z are dimensionless spin operators. The primary function of the large Zeeman Hamiltonian is, of course, to polarize the nuclear magnetic moments to enable a signal to be observed. But because of Condition 2, the wavefunction of the spin system is mainly determined by the Zeeman Hamiltonian. The effect of H_i^{SL} is only to perturb weakly the eigenstates of the Zeeman Hamiltonian. Although the rf field causes a few transitions among the Zeeman states (and thus allows the magnetization of a spin system to be detected), H_{rf} does not significantly alter the eigenstates of the Zeeman and spin-lattice Hamiltonians. A considerable portion of standard textbooks (1,2) is devoted to analyzing NMR spectra in terms of spin-lattice parameters (that is, part 1 of the above experimental strategy). The important point for this discussion is that the structure of a cw NMR spectrum will result from the perturbation (of the Zeeman wavefunctions) by H_i^{SL}, to first and sometimes second order.

Let us now consider multiple pulse NMR. It will be shown that

multiple pulse NMR experiments increase the possible methods of measuring the spin-lattice coupling parameters. In these experiments, the radio-frequency field is adjusted to be much stronger than the spin-lattice interactions.

$$H_o^L >> H_o^S >> H_{rf} >> H_i^{SL} \tag{5}$$

Furthermore, H_{rf} can have a rather complicated form even in the rotating frame

$$H_{rf}(t) = - h\omega_1(t)[I_x \sin\phi(t) + I_y \cos\phi(t)] \tag{6}$$

where both the phase, ϕ, and the amplitude, ω_1, may now be strongly time dependent. The eigenstates of a spin system will still be primarily determined by the Zeeman Hamiltonian. However, because the rf perturbation is strong and its frequency close to resonance, the time development of the spin system will be altered. H_i^{SL} will act as a perturbation, not upon the simple eigenstates of the Zeeman Hamiltonian as before, but upon this time development of a spin system due to the rf field. The effect of the spin-lattice couplings upon the time development of a spin system due to the rf field may be described approximately by the time development operator

$$U^{SL}(t) = \exp(-i\textstyle\sum_i \alpha_i H_i^{SL} t) \tag{7}$$

where α_i is a scaling factor. The significance of multiple pulse NMR is that H_{rf} can often be adjusted, by choosing $\omega_i(t)$ and $\phi(t)$ appropriately, so that each α_i can have any value between 0 and 1.

An elegant formalism, known as Average Hamiltonian Theory, has been

worked out (3,4) to calculate the perturbation of the time development of the spin system as described above. It has successfully predicted not only the gross features of multiple pulse NMR spectra, but also most of the fine details (see Chapter 2 and references therein). Also note that multiple pulse NMR is regarded by this author in a general sense to include any experiment in which the large rf field selects the nature of the effects of H_i^{SL} on the spin system, whereas other authors often just consider it to include the "Waugh cycles" exclusively.

Having set the stage in the preceding paragraphs, question 1 can now be answered. Multiple pulse NMR can be used to advantage in two ways.

Consider the case where several spin-lattice Hamiltonians are present simultaneously, but one is much larger than the others. Conventional cw NMR experiments usually only furnish the measurement of the parameter belonging to this largest coupling because this coupling will dominate the observed spectrum. On the other hand, by using multiple pulse NMR, the rf field can often be applied in a manner such that the largest interaction is completely suppressed so that the remaining spin-lattice interactions will dominate the multiple pulse spectra. More spin-lattice parameters can be retrieved using multiple pulse techniques and hence the lattice can be better characterized. This point is further explored in the answer to question 3 and in Chapter 3.

Now consider a physically complicated, uncharacterized lattice. Although a cw spectrum may be easy to obtain, there may be no obvious physical basis on which to decide which spin-lattice couplings control the observed spectrum. Because the spectra of different multiple pulse experiments can be sensitive to different spin-lattice couplings,

these experiments can be used to detect and to verify the presence of certain types or classes of spin-lattice interactions. Thus multiple pulse NMR can aid the elucidation of cw spectra. Application of this procedure is discussed in the answer to question 4 and in Chapter 4.

ANSWER TO QUESTION 2

Although the initial application (3,4) of Average Hamiltonian Theory successfully explained the basic character of the spectra observed in multiple pulse NMR, many details and anomalies remained a mystery. Because several thousand rf pulses are applied in a time span of milliseconds to obtain a single multiple pulse spectrum, the cumulative effect of even small pulse errors was suspected as being responsible for these unexplained phenomena. Previous studies had attempted to analyze some of these effects, but had had only very limited success (see Chapter 2 and references therein).

A thorough investigation of the effects of pulse errors is presented in Chapter 2. This chapter includes not only a general theoretical method and detailed calculations but also substantial experimental verification. The first step, in order to analyze the effects of pulse errors, is to divide the rf Hamiltonian into two parts.

$$H_{rf} = H_{rf}^{0} + H_{rf}^{1} \tag{8}$$

H_{rf}^{0} is chosen so that it satisfies the periodic and cyclic conditions of Average Hamiltonian Theory (4). Under these conditions, H_{rf}^{0} is called the ideal portion of the rf Hamiltonian. H_{rf}^{1} is called the nonideal portion since it is the difference between the real rf Hamiltonian and

the ideal rf Hamiltonian. The following assumption is made

$$H_{rf}^{0} >> H_{rf}^{1} \tag{9}$$

Because of Condition 9, the time development of a spin system is primarily due to H_{rf}^{0}. The nonideal rf Hamiltonian can be treated as a perturbation of the time development of a spin system due to H_{rf}^{0} just as the spin-lattice couplings are also treated as perturbations of the time development of a spin system due to H_{rf}^{0}. Thus the entire character of the problem of treating nonideal rf fields is identical to that treated previously (3,4) and therefore the same elegant Average Hamiltonian formalism can be used. Because the Average Hamiltonian Theory is simple, systematic, and straightforward, the treatment of pulse imperfections is also simple, systematic, and straightforward.

ANSWER TO QUESTION 3

In solids the large dipolar interactions among the nuclear spins often mask the small chemical shift interactions. However, by applying appropriate multiple pulse cycles (5,6), the dipolar Hamiltonian may be suppressed and the chemical shift tensor retrieved. The principal values of the chemical shift tensor can be obtained by simply measuring the multiple pulse spectrum as a function of orientation of the crystal with respect to the applied field. Further details are discussed in Chapters 3, 4, and references listed therein. Note that in liquids the dipolar Hamiltonian is averaged to zero by the rapid and random motions of the molecules. These same motions, however, also average the chemical shift tensor so that only the isotropic portion is observed.

The chemical shift tensor was measured for $Ca(OH)_2$. The results of this measurement are presented and discussed in Chapter 3. $Ca(OH)_2$ is of particular interest because it represents a model system of non-hydrogen-bonded hydroxyl groups.

The measurement of the proton chemical shift tensor of $Ca(OH)_2$ was a test case for the applicability of multiple pulse NMR techniques. In $Ca(OH)_2$, there is a strong dipolar coupling among the protons. (The wide line spectrum is about 10 gauss full-width at half-height.) The resolution of multiple pulse NMR experiments had been typically poor for systems with a large dipolar Hamiltonian (3-6). However, improvements, which have been made in the design of the sample probe and receiver, enable measurement of the chemical shift tensor even under the adverse condition of strong dipolar coupling such as in $Ca(OH)_2$. Details of the equipment modifications are described in Chapter 4.

ANSWER TO QUESTION 4

The primary experimental problem with NMR studies of adsorption is the marginal signal-to-noise ratio. This difficulty had been partially circumvented by most earlier investigators by studying physically adsorbed systems rather than chemisorbed systems. Physically adsorbed systems give larger signals due to the greater number of nuclei present. Furthermore, noise for physically adsorbed systems can be reduced because they usually have longer T_2's (hence filters with longer time constants may be used). Physically absorbed systems also usually have shorter T_1's (hence more signal averaging may be used during a given period of time).

In the study presented in Chapter 4 of chemisorbed hydroxyl groups

on silica-aluminas, none of these factors are available, so that this signal-to-noise problem is particularly aggravated. Essentially, the signal-to-noise problem was overcome in this investigation by brute force. Surfaces of exceptionally high area, 600 m^2/gm, were used. Extensive signal averaging was employed (256 decays which took 4 hours and 16 minutes). Finally, because the spectrometer had been designed to meet the stringent requirements for multiple pulse NMR, it easily met the requirements for the simple free induction decay experiments which comprise the bulk of the data presented in Chapter 4. Multiple pulse experiments were also possible because, as pointed out in Chapter 2, the eight-pulse cycle has exceptionally good stability. Other experimental factors are discussed in Chapter 4.

The primary theoretical problem of NMR studies of adsorption is interpreting the free induction decay spectra, because several spin-lattice coupling terms can be present simultaneously. In this connection, multiple pulse NMR proved to be indispensable. For example, because the eight-pulse cycle narrowed the line observed from protons on pure silica, the exponential shape of the free induction decay would be ascribed to the static proton-proton dipolar interaction rather than random motional effects. Furthermore, because the eight-pulse cycle narrowed the line observed from protons on 90% and 75% silica, the shape of the free induction decay would be ascribed to the proton-proton dipolar interaction rather than the proton-aluminum coupling. The Meiboom-Gill cycle was employed both to prove the presence of and to measure the proton-aluminum dipolar broadening on other samples. Thus, multiple pulse NMR was effectively used to sort out possible spin-lattice interactions in this complicated adsorption system.

REFERENCES

1. Slichter, C. P., "Principles of Magnetic Resonance," Harper and Row, New York, 1963.

2. Abragam, A., "The Principles of Nuclear Magnetism," Oxford University Press, London, 1961.

3. Evans, W. A. B., Ann. Phys. (N. Y.) 48, 72(1968).

4. Haeberlen, U., and Waugh, J. S., Phys. Rev. 175, 453(1968).

5. Waugh, J. S., Huber, L. M., Haeberlen, U., Phys. Rev. Lett. 20, 180(1968).

6. Rhim, W. -K., Elleman, D. D., and Vaughan, R. W., J. Chem. Phys. 58, 1772(1973); Rhim, W. -K., Elleman, D. D., Vaughan, R. W., J. Chem. Phys. 59, 3740(1973).

CHAPTER 2

ANALYSIS OF MULTIPLE PULSE NMR IN SOLIDS. II.

(The text of Chapter 2 consists of an article coauthored with W.-K. Rhim, D. D. Elleman, and R. W. Vaughan that has appeared in Journal of Chemical Physics, Vol. 60, No. 11, 1 June 1974.)

INTRODUCTION

Multiple pulse nuclear magnetic resonance (NMR) techniques have been successfully developed and applied during the past few years (1-16). Of particular interest, has been the development of methods of suppressing the effects of homonuclear dipolar broadening and thus obtaining high resolution NMR spectra of solids. A theoretical framework which is well adapted for discussing these techniques has been developed (2,5,13,15), and accounts for much of what is experimentally observed. However, the multiple pulse NMR techniques have been handicapped from the beginning (11,12,14,15,17) because of the presence of a number of characteristics which would frequently appear in the spectra such as overall frequency shifts, non-linearities in the scaling of chemical shifts, and the often puzzling nature of second averaging.

As one applies up to several thousand rf pulses in a time span of milliseconds to obtain a single spectrum, it has often been speculated that the cumulative effect of even small pulse errors could be responsible for these unexplained phenomena. Although a number of articles have appeared which have attempted to analyze some of the effects of pulse nonidealities (14,15,17,18), no general method has been proposed which could successfully explain the multitude of effects that small pulse errors can produce. It is the purpose of this paper to demonstrate that a number of pulse imperfections (phase errors, length errors, rf inhomogeneity, and phase transient effects) can be quite generally incorporated into the average Hamiltonian formulation (2-4). It is shown that it is not only possible to calculate an average Hamiltonian for the pulse imperfections but also straightforward to calculate the coupling terms of the pulse imperfections

with other components of the Hamiltonian such as the dipolar and off resonance terms. This treatment presents a simple geometric picture of the effects of pulse imperfections and explains many of the features of spectra obtained with an improperly tuned spectrometer. Knowledge of the coupling terms between pulse errors and other components of the Hamiltonian such as the dipolar and off resonance terms will be shown to explain how specific pulse errors affect the experimental resolution.

The formalism developed here is applied to four different pulse cycles of importance to the homonuclear multiple pulse NMR techniques and the results are presented in Tables I and II. Experimental verification of both the qualitative and quantitative correctness of the calculated average Hamiltonians for pulse length errors, pulse phase errors, and phase transient effects are obtained within the framework of the flip-flop cycle. The effects of two higher order correction terms are measured and found to agree with predictions for the $90_x - 90_x - 90_x - 90_x$ cycle.

Finally, the results of this analysis are used to discuss the proper methods of experimentally detecting and removing pulse imperfections and the relative merits of the four pulse and the eight pulse cycles with respect to pulse imperfections. The effects of rf power droop on these pulse cycles are given in the Appendix.

THEORY

First, we briefly review the average Hamiltonian concept (2-4). The rotating frame Hamiltonian commonly encountered in homonuclear solid state NMR studies can be written as

$$H(t) = H_{rf}(t) + H_{int} \tag{1}$$

where $$H_{int} = H_0 + H_D^{(z)} \tag{2}$$

The $H_{rf}(t)$ depends on the nature of the rf excitation applied to the sample while the offset Hamiltonian, H_0, composed of chemical shift and off-resonance terms, and the dipolar interaction, $H_D^{(z)}$, have the following forms:

$$H_0 = (\omega - \omega_\circ)I_z + \omega_\circ \Sigma_i \sigma_{zzi} I_{zi} = \Sigma_i \left(\Delta\omega + \omega_\circ \sigma_{zzi}\right) I_{zi} \tag{3}$$

$$H_D^{(z)} = \Sigma_{i<j} \Sigma B_{ij} \left(\frac{r}{-ij}\right) \left(\underline{I}_i \cdot \underline{I}_j - 3I_{zi}I_{zj}\right) \tag{4}$$

H_{int} is time independent while $H_{rf}(t)$ is strongly time dependent for the rf pulse trains used in multiple pulse experiments. Since $H_{rf}(t)$ is the major perturbation, the time development operator can be written (19)

$$U(t) = U_{rf}(t) U_{int}(t) \tag{5}$$

where $$U_{rf}(t) = \mathsf{T} \exp\left[-i \int_o^t H_{rf}(t')dt'\right] \tag{6}$$

$$U_{int}(t) = \mathsf{T} \exp\left[-i \int_o^t \tilde{H}_{int}(t')dt'\right] \tag{7}$$

$$\tilde{H}_{int}(t) = U_{rf}^{-1}(t) H_{int} U_{rf}(t) \tag{8}$$

and T is the Dyson time ordering operator. If $H_{rf}(t)$ satisfies periodic and cyclic conditions (4) then $\tilde{H}_{int}(t)$ becomes periodic as well, and one only needs to calculate $U_{int}(t)$ for a single cycle in order to be able to predict

the time development of the spin system at integral multiples of the cycle time; i.e. one requires over a time t_c:

$$H_{rf}\left(t + Nt_c\right) = H_{rf}(t) \qquad \text{(periodic condition)} \tag{9}$$

and $$U_{rf}\left(Nt_c\right) = \mathbf{T}\exp\left[-i\int_0^{Nt_c} H_{rf}(t')dt'\right] = 1 \qquad \text{(cyclic condition)} \tag{10}$$

and then

$$U_{int}\left(Nt_c\right) = \left[U_{int}\left(t_c\right)\right]^N \tag{11}$$

Now $U\left(t_c\right)$ can be expanded using the Magnus formula (20),

$$U_{int}\left(t_c\right) = \exp\left[-i\, t_c\left(\bar{H}_{int}^{(0)} + \bar{H}_{int}^{(1)} + \bar{H}_{int}^{(2)} + \ldots\right)\right] \tag{12}$$

where $$\bar{H}_{int}^{(0)} = \frac{1}{t_c}\int_0^{t_c} \tilde{H}_{int}(t')dt' \tag{13}$$

$$\bar{H}_{int}^{(1)} = \frac{-i}{2t_c}\int_0^{t_c} dt_2 \int_0^{t_2} dt_1\left[\tilde{H}_{int}\left(t_2\right), \tilde{H}_{int}\left(t_1\right)\right] \tag{14}$$

$$\bar{H}_{int}^{(2)} = \frac{1}{6t_c}\int_0^{t_c} dt_3 \int_0^{t_3} dt_2 \int_0^{t_2} dt_1 \left\{\left[\tilde{H}_{int}\left(t_3\right), \left[\tilde{H}_{int}\left(t_2\right), \tilde{H}_{int}\left(t_1\right)\right]\right] + \left[\tilde{H}_{int}\left(t_1\right), \left[\tilde{H}_{int}\left(t_2\right), H_{int}\left(t_3\right)\right]\right]\right\} \tag{15}$$

The convergence condition for Eq. (12) is roughly

$$t_c \,||\, \tilde{H}_{int}(t) \,|| \ll 1 \tag{16}$$

where $||\, \tilde{H}_{int}(t) \,||$ is the magnitude of $\tilde{H}_{int}(t)$. Thus there are three conditions which must be met by $H_{rf}(t)$: (i) the periodic condition of Eq. (9), (ii) the cyclic condition of Eq. (10), and (iii) the convergence condition of Eq. (16).

The Treatment of Non-ideal rf Perturbations

Although the idealized representation of the pulse cycles commonly used in multiple pulse NMR studies satisfies the cyclic, periodic, and convergence conditions listed above, the pulse cycles which are applied in an actual experiment may not. A number of commonly encountered pulse imperfections may produce violation of the cyclic condition such as phase transients, phase misadjustments, and errors in pulse length. (It should be noted that for phase alternated cycles the introduction of rf inhomogeneity does not produce violation of the cyclic and periodic conditions, and the reader is referred to previous work (15b) for a detailed discussion of the effects of this particular pulse imperfection.) In cases where pulse imperfections cause weak violations of the cyclic condition, it will be shown below that the problem can still be treated in a general fashion by redefining $H_{int}(t)$ in such a way as to include the non-cyclic portion of the experimental $H_{rf}(t)$. The effects of rf power droop, which causes violation of both the cyclic and periodic conditions, are discussed in the Appendix.

If $H_{rf}(t)$ satisfies the periodic condition, but because experimental errors or misadjustments fails to satisfy the cyclic condition, one can divide it into two parts, i.e.

$$H_{rf}(t) = H^0_{rf}(t) + H^1_{rf}(t) \tag{17}$$

where $H^0_{rf}(t)$ represents the ideal pulse cycle which satisfies both periodic and cyclic conditions and $H^1_{rf}(t)$ represents the non-ideal portion of the rf pulses. We assume that the following relation is satisfied between these two terms,

$$|| H^0_{rf}(t) || >> || H^1_{rf}(t) || \tag{18}$$

One can then combine $H^1_{rf}(t)$ with H_{int} in Eq. (1) and then repeat all the steps in the previous section to calculate the average Hamiltonian, $\bar{H}^{(0)}_{int}$, and its correction terms. In general one may write $H^1_{rf}(t)$ as a sum of Hamiltonians of the individual imperfections present, i.e.

$$H^1_{rf}(t) = \sum_k H_k(t) \tag{19}$$

In the following applications, k will represent, for example, P for phase misadjustments, T for phase transients, δ for pulse length misadjustments, and ε for rf inhomogeneity. Then the average Hamiltonians take the form:

$$\bar{H}^{(0)}_{int} = \bar{H}^{(0)}_0 + \bar{H}^{(0)}_D + \sum_k H^{(0)}_k \tag{20}$$

$$\bar{H}^{(1)}_{int} = \bar{H}^{(1)}_0 + \bar{H}^{(1)}_D + \bar{H}^{(1)}_{0D} + \sum_k \left(\bar{H}^{(1)}_{0k} + \bar{H}^{(1)}_{Dk} \right) \tag{21}$$

$$\bar{H}^{(2)}_{int} = \bar{H}^{(2)}_0 + \bar{H}^{(2)}_D + \bar{H}^{(2)}_{0D} + \sum_k \left(\bar{H}^{(2)}_{0k} + \bar{H}^{(2)}_{Dk} \right) \tag{22}$$

The nomenclature here is straightforward with, for instance, $H^{(1)}_{0k}$ representing the first order coupling between resonance offset, H_0, and the k-th imperfection, $H_k(t)$. Cross terms generated by interaction of two imperfections have been neglected in Eqs. (21) and (22) as $H^1_{rf}(t)$ will in general be much smaller than H_{int} for the applications presented here. These terms should, of course, be added in other applications where they could be significant.

Colloquially speaking then, it is thus possible to stuff the non-cyclic portion of the rf perturbation into the internal Hamiltonian. This method will be demonstrated below to offer distinct advantages over previous treatments (12,14,17,18) because (i) a large class of pulse imperfections can be examined directly, (ii) the analytical form allows pulse cycle

imperfections to be treated in a general fashion, and (iii) it is possible to use the formulation of the average Hamiltonian treatment to sort out and understand the detailed physics of the interactions of pulse trains which have several types of imperfections present simultaneously.

DISCUSSION OF RESULTS

Four different pulse cycles of particular importance to the development of the multiple pulse techniques for solid state NMR studies are shown in Figure 1. The $90_x - 90_x - 90_x - 90_x$ and flip-flop sequences are used in tuning the multiple pulse spectrometer. The $90_x - 90_x - 90_x - 90_x$ sequence is used to adjust pulse lengths precisely and allows a direct measurement of rf inhomogeneity (12,15b), while the flip-flop sequence (21) is used to obtain a 180° phase difference between two pulses and provides a means of measuring phase transient effects (12,14). Both the four pulse sequence (1) and eight pulse sequence (15a) are used to suppress homonuclear dipolar and quadrapolar broadening.

Pulse non-idealities which satisfy the cyclic condition and which will be explicitly considered are: rf inhomogeneity, errors in pulse shape and in pulse size (either height or width), phase errors, and effects of phase transients. The rf Hamiltonian for an x pulse then becomes in the form of Eqs. (17) and (19):

$$\mathcal{H}_{rf}(t) = -\omega_1 I_x - \sum_i \frac{\epsilon_i}{t_w} I_{xi} - \frac{\delta_x}{t_w} I_x - \omega_1 \sin\phi_x I_y - \omega_I(t) I_x + \omega_T(t) I_y \quad (23)$$

where the conditions,

$$\left|\frac{\epsilon_i}{t_w}\right|, \left|\frac{\delta_x}{t_w}\right|, \left|\phi_x \omega_1\right|, \left|\omega_I(t)\right|, \left|\omega_T(t)\right| \ll \left|\omega_1\right| \quad (24)$$

are assumed to be satisfied. In Eq. (23): (i) $\omega_1 I_x = \mathcal{H}^0_{rf}(t)$ represents the ideal rectangular x pulse $\left(\text{of width } t_w\right)$, (ii) ϵ_i is the error in rotation angle of a pulse at the i'th nucleus caused by rf inhomogeneity and is defined so that

$$\sum_i \epsilon_i = 0 \quad (25)$$

where the summation is over all nuclei in the sample, (iii) δ_x is a pulse

size misadjustment, (iv) ϕ_x is a phase angle misadjustment, (v) $\omega_I(t)$ is defined as the difference between the in phase component of the real rf pulse and the idealized rectangular pulse defined in (i). The condition

$$\int_0^{t_w} \omega_I(t)dt = 0 \tag{26}$$

is imposed, (vi) $\omega_T(t)$ defines the amplitude of the signal orthogonal in phase to the idealized pulse, defined in (i) and thus represents the phase transient phenomena. Without any loss in generality the condition

$$\int_0^{t_w} \omega_T(t)dt = 0 \tag{27}$$

is imposed on the transient.

One should note that the choice of a specific value for the idealized pulse width, t_w, is not clearly defined by experiment because of the time dependent quantities $\omega_I(t)$ and $\omega_T(t)$. Here t_w is chosen such that Eq. (24) is satisfied during the ideal pulse and such that $\omega_I(t)$ and $\omega_T(t)$ may be neglected outside the ideal pulse. Furthermore, t_w is chosen such that $t_w/t_c \ll 1$. Thus although the average Hamiltonians appearing in Tables I II include effects of pulses of finite width, pulses are approximated as delta functions for the calculation of the higher order correction terms. If these conditions cannot be met experimentally, calculations may be necessary of additional higher order correction terms to the average Hamiltonian and of the effects of pulses of finite width on higher order terms.

With the general assumptions listed above and the condition of Eq. (26), the effect of the non-rectangular shape of the pulse, $\omega_I(t)I_x$, was found to vanish. Consequently no further reference will be made to this pulse error.

The Flip-Flop and $90_x - 90_x - 90_x - 90_x$ Pulse Sequences

Because of their simplicity the $90_x - 90_x - 90_x - 90_x$ and flip-flop sequences will be discussed first and the results compared with experimental data to verify the applicability of the theoretical approach described above. Table I contains the results for the pulse imperfections of Eq. (23) for the flip-flop cycle, $\left\{\tau - \left(\frac{\pi}{2}\right)_x - 2\tau - \left(\frac{\pi}{2}\right)_{-x} - \tau\right\}^N$. Here we have assumed that the sample will be a liquid which will produce only one absorption line and hence may write $\sigma_{zzi} = 0$ for all spins.

A simple geometric description of the time development of the magnetization is obtained by observing in Table I that all of the Hamiltonians of pulse imperfections contribute terms which are linear in the spin operators, and hence the Hamiltonians transform under rotation as vector operators. The resultant Hamiltonian is obtained by adding the separate terms in Table I, and if one ignores the rf inhomogeneity term for the present, the resultant Hamiltonian can be expressed,

$$\bar{H}_{int} = \underline{\Omega} \cdot \underline{I} \tag{28}$$

We then have formally for the time development of the magnetization

$$\langle \underline{M}(Nt_c) \rangle = Tr\left\{\underline{M}\, U(Nt_c)\, \rho(0) U^{-1}(Nt_c)\right\} \tag{29}$$

where $U(Nt_c)$ is given by Eqs. (11) and (12) and $\rho(0)$ is the initial density matrix. On the other hand, Eq. (28) can be interpreted geometrically as causing the coherent precession of the initial magnetization, $\underline{M}_0$, around a vector, $\underline{\Omega}$, with angular frequency $|\underline{\Omega}|$, and thus the calculation of the time dependence of the magnetization becomes a trivial operation. This nomenclature will be used whenever it is appropriate below and $\underline{M}_0$ and $\underline{\Omega}$ will

be given rather than stating the time dependence of each component of the magnetization.

The results in Table I are for the flip-flop cycle, $\left\{\tau - \left(\frac{\pi}{2}\right)_x - 2\tau - \left(\frac{\pi}{2}\right)_{-x} - \tau\right\}^N$ and should thus be compared with the experimentally measured magnetization after the -x pulse. It is also clear that experimentally one can measure the magnetization after the +x pulse as well. One must, however, use a redefined cycle,

$$\tau - \left(\frac{\pi}{2}\right)_x - \tau - \left[\tau - \left(\frac{\pi}{2}\right)_{-x} - 2\tau - \left(\frac{\pi}{2}\right)_x - \tau\right]^{N-1}$$

and repeat the calculations to predict the behavior of the magnetization in this window, as it will in general be different.

Figures 2a-e show experimental data obtained for the flip-flop cycle as specific pulse errors were systematically introduced. Because the photographs in Figs. 2a-e show the magnetization in both windows, results and discussion are presented in this section for both forms of the cycle (although $\bar{H}^{(0)}_{int}$ and its correction terms are reported in Table I only for the cycle shown in Fig. 1a).

Figure 2a shows the magnetization for a properly tuned spectrometer but where an inhomogeneity in the magnetic field, H_o, has been deliberately introduced, causing the slight decay in the upper trace of Fig. 2a. The spectrometer was tuned following the procedure previously published (12). As this is the on resonance case with no pulse imperfections the calculated results are simply (ignoring the magnetic field inhomogeneity)

$$\underline{M}_o = M_o\underline{k}, \quad \underline{\Omega} = 0 \text{ for magnetization sampled after -x pulses} \tag{30}$$

$$\underline{M}_o = M_o\underline{j}, \quad \underline{\Omega} = 0 \text{ for magnetization sampled after x pulses} \tag{31}$$

where $\underline{i}$, $\underline{j}$, and $\underline{k}$ are unit vectors pointing along the x, y and z axis of the

rotating frame. The phase detector has been adjusted to sample the component of the magnetization along the y, or $\underline{j}$, axis. The upper trace is the magnetization sampled after the x pulses while the lower trace is the magnetization sampled after the -x pulses.

Figure 2b illustrates the results obtained by going off resonance with a well tuned spectrometer. Going off resonance an amount, $\Delta\omega$, requires the introduction of the effect of the resonance offset Hamiltonian, $\bar{H}_0^{(0)}$, and from Table I the evolution of the magnetization following the -x pulses can be calculated:

$$\underline{M}_o = M_o\underline{k}, \quad \underline{\Omega} = \frac{\Delta\omega}{2}(1 + 2a/3)(-\underline{j} + \underline{k}) \tag{32}$$

and the signal observed during the alternate windows is calculated to be

$$\underline{M}_o = M_o\underline{j}, \quad \underline{\Omega} = \frac{\Delta\omega}{2}(1 + 2a/3)(\underline{j} + \underline{k}) \tag{33}$$

where $a = \frac{3t_w}{t_c}\left(\frac{4}{\pi} - 1\right)$. The frequency had been changed by 1000Hz for the case illustrated in Fig. 2b and measurement of the frequency of the oscillation in Fig. 2b indicated a scaling factor of 1.36 which compares favorably with 1.38, calculated from Eqs. (32) and (33), i.e.

$$\frac{\Delta\omega}{|\underline{\Omega}|} = \frac{\sqrt{2}}{1 + 2a/3} \tag{34}$$

Figure 2c illustrates the effect of introducing a small phase error, ϕ_x, in the +x pulse at exact resonance. Using the average Hamiltonian for a phase error in Table I, $\bar{H}_P^{(0)}$, one predicts the magnetization following the -x pulses to be

$$\underline{M}_o = M_o\underline{k}, \quad \underline{\Omega}_p = \frac{-\phi_x}{t_c}(\underline{j} + \underline{k}) \tag{35}$$

For the magnetization following the +x pulse, one calculates,

$$\underline{M}_o = M_o \underline{j}, \quad \underline{\Omega}_p = \frac{-\phi_x}{t_c} (\underline{j} - \underline{k}) \tag{36}$$

An experimental phase error of approximately 5° was introduced and using Fig. 2c and Eqs. (35) and (36) one predicts a phase error of 5.4°.

One observes that Fig. 2c does not exhibit the decaying envelopes of Figs. 2a and 2b. The decay of magnetization in Figs. 2a and 2b was due to a deliberately introduced inhomogeneity in H_o and its removal is an example of the second averaging effect due to the pulse imperfection Hamiltonian (the phase error Hamiltonian for the present case). In terms of the pertinent Hamiltonians the magnetic field inhomogeneity can be expressed,

$$H_\alpha = \sum_i \alpha_i I_{zi} \tag{37}$$

and with the flip-flop sequence of Table I one obtains the following average Hamiltonian

$$\bar{H}_\alpha^{(0)} = \sum_i \underline{\Omega}_{\alpha_i} \cdot \underline{I}_i \tag{38}$$

where $\underline{\Omega}_{\alpha_i} = \frac{\alpha_i}{2}\left(1 + \frac{2}{3}a\right)(-\underline{j} + \underline{k})$.

The resultant average Hamiltonian for both the effects of the phase error and magnetic field inhomogeneity can be obtained by simply vectorially adding the two effective Hamiltonians [Eq. (20)]. We note here that $\underline{\Omega}_p$ of Eq. (35) and $\underline{\Omega}_{\alpha i}$ are perpendicular to one another and that $\left|\underline{\Omega}_p\right| >> \left|\underline{\Omega}_{\alpha i}\right|$. Thus the magnetic field inhomogeneity will vanish due to second averaging. An appreciation of the simplifying effect of the average Hamiltonian approach to these problems can be obtained by noting the description of Mansfield et al. (14) for similar observations.

Fig. 2d illustrates the effect of adding a pulse length error to the case of Fig. 2a, a properly tuned spectrometer with an H_o field

inhomogeneity. In the case of the example in Figure 2d the x pulse was decreased in size slightly and one needs the effective Hamiltonian for pulse errors from Table I, $\bar{H}_{\delta}^{(0)}$, in order to describe the signal seen following the -x pulses (ignoring the field inhomogeneity for the present),

$$\underline{M}_o = M_o \underline{k}, \text{ and } \underline{\Omega}_{\delta} = \frac{-\delta_x}{t_c} \underline{i} \tag{39}$$

Similarly the signal observed following the +x pulses can be described,

$$\underline{M}_o = M_o \underline{j}, \text{ and } \underline{\Omega}_{\delta} = \frac{-\delta_x}{t_c} \underline{i} \tag{40}$$

Experimentally δ_x was set near -5.8° and the number obtained from Fig. 2d agrees with this. Again the pulse imperfection Hamiltonian, $\bar{H}_{\delta}^{(0)}$, results in a rotation vector Eq. (39) perpendicular to that produced by the distribution of resonance frequencies induced by the magnetic field inhomogeneity [Eq. (38)] and if $\left|\underline{\Omega}_{\delta}\right| >> \left|\underline{\Omega}_{\alpha i}\right|$, one expects to see the effects of the magnet inhomogeneity disappear.

If one alters the tuning of the final rf circuitry such that a phase transient effect is introduced (12,17),one obtains the results shown in Fig. 2e. Again the conditions of Fig. 2a were chosen as the starting point, a well tuned spectrometer, signal on resonance, and the presence of an H_o magnetic field inhomogeneity. Again one obtains the appropriate Hamiltonian, $\bar{H}_T^{(0)}$, for phase transients from Table I and obtains the following description of the magnetization sampled after the -x pulses,

$$\underline{M}_o = M_o \underline{k}, \quad \underline{\Omega}_T = \frac{J_1}{t_c} (-\underline{j} + \underline{k}) \tag{41}$$

following the +x pulses,

$$\underline{M}_o = M_o \underline{j}, \quad \underline{\Omega}_T = \frac{J_1}{t_c} (\underline{j} + \underline{k}) \tag{42}$$

where $J_1 = \int_0^{t_w} \omega_T(t) (\sin \omega_1 t - \cos \omega_1 t) dt$ (43)

Here it is assumed, as has been experimentally verified, [for the instrumentation used here (12)], that the phase transient is repretitive, i.e. no significant random component, and the same for each rf pulse regardless of its rf phase. We note here that the same integral J_1 appears for all 90° pulse, phase alternated, cycles. The fact that J_1 has the same value for all such cycles allows the relatively simple flip-flop cycle to be used to measure J_1 under specific experimental conditions, and thus allow prediction of the effects to be expected in more complicated cycles performed with the same spectrometer tuning. As has been observed previously (12), a sufficient condition (though not a necessary condition) to make $\bar{H}_T^{(0)}$ vanish is that $\omega_T(t)$ is symmetric about $t_w/2$. This result is also predicted by Eq. (43).

It should also be noted that the rotation vector for phase transients in the flip-flop pulse sequence is parallel to the rotation vector for the off resonance Hamiltonian, $\bar{H}_0^{(0)}$, and thus the two will add algebraically, preserving the slope of the frequency scaling plot in the presence of phase transistent effects but shifting the ordinate of the line by $\frac{\sqrt{2}\ J_1}{t_c}$. This is experimentally verified as one notes that there is no reduction in the damping of the magnetization in the presence of the phase transient effects (Fig. 2e) when compared with Fig. 2a.

Finally, we point out that the description of phase transient effects presented here contrasts strongly with previous results which predicted, using the present nomenclature, an angular frequency vector parallel to the z-direction in the rotating reference frame (12,17).

Thus for the average Hamiltonians of the flip-flop pulse sequence experimental verification has been presented indicating both the qualitative and quantitative correctness of the theoretical development. It would be difficult, however, to attempt to verify experimentally the correctness of the higher order correction terms as the much stronger $\bar{H}^{(0)}$ terms control the spectra in the flip-flop sequence. However, one notes in Table I that, in the case of the $90_x - 90_x - 90_x - 90_x$ sequence, two cases occur where the zero order Hamiltonians vanish but higher order terms do not. Thus by tuning the spectrometer to minimize $\bar{H}_{\delta}^{(0)}$ and by keeping $\bar{H}_{d}^{(0)}$ and $\bar{H}_{\varepsilon}^{(0)}$ as small as possible, the first order correction term to the off resonance Hamiltonian $\bar{H}_{0}^{(1)}$, and the first order coupling term between the off resonance Hamiltonian and the phase transient Hamiltonian, $\bar{H}_{0T}^{(1)}$, will control the observed magnetization. Using the form for these Hamiltonians in Table I, one predicts a rotation vector,

$$\underline{\Omega}^{(1)} = -\left(\frac{t_c}{16}(\Delta\omega)^2 + \frac{1}{2}\,\Delta\omega\, J_1\right)\underline{i} \tag{44}$$

where J_1 is defined in Eq. (43). Fig. 3 is a plot of $\frac{\Omega^{(1)}}{2\pi}$ for two different values of J_1 and the solid curves are the theoretical prediction from Eq. (44) (using values of J_1 measured with the flip-flop sequence). One notes very good agreement. In addition, values of $\frac{d\Omega^{(1)}}{d(\Delta\omega)}$ were measured at $\Delta\omega = 0$ for several different values of J_1 (again experimentally determined using the flip-flop sequence) and the results are plotted in Fig. 4. One notes the linear function of J_1 obtained and furthermore the slope of the line agrees within a few percent with the prediction,

$$\frac{\left[d\Omega^{(1)}/d(\Delta\omega)\right]_{\Delta\omega = 0}}{\left(\frac{J_1}{\sqrt{2}\pi t_c}\right)} = -\frac{t_c\pi}{\sqrt{2}} \tag{45}$$

where $\frac{J_1}{\sqrt{2}\pi t_c}$ is the frequency at resonance measured from the flip-flop sequence with t_c = 30 μsec. Thus both the qualitative and quantitative correctness of two higher order correction terms has been experimentally verified and further substantiate the correctness of the present treatment.

Procedure for Tuning Spectrometer

Techniques have been previously described (12) which allow one to tune the spectrometer to remove the effects of pulse errors using the $90_x - 90_x - 90_x - 90_x$, the flip-flop, and other simple pulse cycles. The theoretical treatment developed in the previous sections will be applied here to furnish a theoretical justification for this procedure.

The first step is to apply the $90_x - 90_x - 90_x - 90_x$ cycle to a liquid sample in order to adjust the +x pulse sizes to $\pi/2$. As can be seen in Table I $\bar{H}_T^{(0)} = 0$ for this cycle, so that the existence of phase transients at this point will not interfere with the adjustment of the pulses to the proper length. However, $\bar{H}_\varepsilon^{(0)}$, the average Hamiltonian due to rf inhomogeneity, will cause a decay of the magnetization and thus can limit the accuracy with which one can adjust the pulse lengths. This is not a particularly serious limitation as a 1% rf inhomogeneity, (greater than normally obtained), allows an adjustment of the pulse length to within a half of a degree, and in fact use of a more complex pulse sequence $90_x - 90_x - 90_x - 90_x - 90_{-x} - 90_{-x} - 90_{-x} - 90_{-x}$ will remove even this small limitation on pulse length adjustment. The presence of the $\bar{H}_\varepsilon^{(0)}$ can be used to obtain an estimate of the inhomogeneity in the rf magnetic field. For example, if the magnetization decays exponentially with a decay constant of T_2, the fractional rf inhomogeneity is $t_c/\pi T_2$ where t_c in the cycle time containing four $90°_x$ pulses.

After separately adjusting the pulse lengths of the -x and +x pulses to $\pi/2$ one uses the flip-flop cycle to adjust the relative phase between them to 180° and to measure and minimize the phase transient effect. From Table I it is clear that the resultant rotation vectors for all the pulse error Hamiltonians except the phase transient, $\bar{H}_T^{(0)}$, will be perpendicular to the rotation vector for the off resonance Hamiltonian, and consequently, if one observes the magnetization sufficiently far off resonance the effects of these pulse error Hamiltonians will vanish due to second averaging (22). The rotation vector due to the phase transient, $\bar{H}_T^{(0)}$, on the other hand is parallel to that of the off resonance Hamiltonian, $\bar{H}_0^{(0)}$, and its magnitude can be determined by comparing the beating frequency observed above and below resonance. One predicts for example that for an observation $\Delta\omega$ above resonance that the frequency will be,

$$(\Delta\omega/\sqrt{2})(1 + 2a/3) + \sqrt{2}\, J_1/t_c,$$

while for the same amount below resonance the observed frequency will be,

$$(\Delta\omega/\sqrt{2})(1 + 2a/3) - \sqrt{2}\, J_1/t_c.$$

Thus the difference in these two frequencies, $\sqrt{8}\, J_1/t_c$ is a direct measure of the phase transient effect and by adjusting the spectrometer tuning until the two observed frequencies are identical, one can tune out such effects. The following iterative procedure can be followed: (a) adjust the spectrometer tuning such that the beat frequencies observed above and below resonance are identical, (b) readjust the pulse lengths to $\pi/2$ using the $90_x - 90_x - 90_x - 90_x$ cycle, (c) check again to see if phase transient effect is still zero; if not repeat the procedure.

After eliminating the phase transient effect in this fashion one observes the flip-flop sequence on resonance in order to detect any phase

misadjustment between the +x and -x pulses. Since the effects of pulse length errors, $\bar{H}_{\delta}^{(0)}$, and phase transients, $\bar{H}_{T}^{(0)}$, have been removed, any oscillations observed in the magnetization at this point are due to phase errors, $\bar{H}_{P}^{(0)}$. We note for the four pulse and eight pulse cycle that in order to make $\bar{H}_{P}^{(0)}$ vanish, one must carefully adjust the phases with the flip-flop cycle to obtain the condition $\phi_x - \phi_{-x} = 0$.

The only additional steps necessary to complete the tuning of the spectrometer for use of the four and eight pulse cycles involve the adjustment of the y and -y pulses to the proper length and phase. The first step is to adjust the length of the y and -y pulses to $\frac{\pi}{2}$. Then the 90° phase difference between the +x and +y pulses is set with a $90_x - 90_y - 90_x - 90_y - 90_x - 90_y$ cycle as previously described (12). The flip-flop sequence is then used to set the 180° phase difference between the +y and -y pulses, which will then make $\bar{H}_{P}^{(0)}$ vanish for the four pulse and eight pulse cycles, thereby completing the procedure. The theoretical treatment developed here thus explains how the previously described tune-up procedure allows separation of the effects of various pulse errors which are present simultaneously and provides a straightforward means of properly adjusting the spectrometer.

The Four and Eight Pulse Cycles

The effects of pulse imperfections on two different pulse cycles which are used to greatly reduce the effects of homonuclear dipolar broadening are presented in Table II. The four pulse cycle of Waugh, Huber, and Haeberlen (1) is compared with the eight pulse cycle recently shown (15a) to offer significantly improved resolution. Portions of the results in Table II have

been reported and discussed previously, and in particular, the reader is referred to the paper of Rhim, Elleman, and Vaughan (15b) for a discussion of rf inhomogeneity effects and to papers of Waugh and co-workers (3,4) for a discussion of the idealized pulse Hamiltonians and to Mansfield's work (13) on compensation of pulse cycles to eliminate the effects of some pulse imperfections.

No attempt will be made to discuss in a comprehensive fashion all of the information contained in Table II. However, a few specific examples will illustrate how the information contained in Table II can be applied to sorting out and understanding the complexitites produced by pulse imperfections.

As the largest term in the Hamiltonians is likely to be the dipolar interaction its first order coupling terms with the pulse errors can easily prove to limit the experimental resoltuion. In the case of the four pulse cycle the situation is rather complex as even the zeroth order dipolar term $\bar{H}_D^{(0)}$ is non-zero and pulse errors in phase, amplitude, or inhomogeneity can all produce sizable terms as indicated in Table II.

On the other hand for the eight pulse cycle, not only does $\bar{H}_D^{(0)}$ vanish but $\bar{H}_D^{(1)}$ vanishes also (even considering pulses of finite width). In addition, the first order couplings of the dipolar Hamiltonian with phase errors, phase transients, pulse amplitude errors, and rf inhomogeneity all vanish. Thus these pulse errors are not expected to affect the resolution in the eight pulse cycle nearly as severely as they do in the four pulse cycle. An experimental comparison of these two cycles confirms this and provides data to indicate that small instrumental fluctuations had much greater effect on the resolution in the four pulse cycle than in the eight pulse cycle (15b).

Further differences between the four pulse and eight pulse cycles are exhibited in their respective chemical shift scaling plots. The theoretical analysis of these ideal pulse cycles predicts that the chemical shift scaling curves should be linear. Thus the linearity of a scaling curve has often been used as a justification that the spectrometer is properly tuned (11,12). Indeed one finds from Table II that the average Hamiltonians of pulse errors in phase and pulse length can produce non-linear curves for both the four pulse and the eight pulse cycle. However, although the average Hamiltonian for a phase transient $\bar{H}_T^{(0)}$ can cause a non-linear scaling curve for the four pulse cycle, we see that $\bar{H}_T^{(0)}$ for the eight pulse cycle will not destroy the linearity because $\underline{\Omega}_T^{(0)}$ is parallel to $\underline{\Omega}_0^{(0)}$. However, for the eight pulse cycle, a phase transient will cause the observed frequencies to be shifted an amount $\left|\underline{\Omega}_T^{(0)}/2\pi\right|$.

Experimental confirmation of this prediction for the four pulse cycle is illustrated in Fig. 5 which shows the chemical shift scaling curve for two values of J_1, one of them being very close to zero. The $J_1 \approx 0$ case is linear within the accuracy of the measurements while the curvature of the $J_1 \neq 0$ case is evident. In these plots the points are experimental while the curves are obtained from the following equation

$$\left|\frac{\underline{\Omega}}{2\pi}\right| = \frac{1}{2\pi}\left|\underline{\Omega}_0^{(0)} + \underline{\Omega}_T^{(0)}\right| = \left[2\left(\frac{1+a}{3}\Delta\nu + \frac{J_1}{2\pi t_c}\right)^2 + \left(\frac{1+a}{3}\Delta\nu + \frac{J_1}{\pi t_c}\right)^2\right]^{1/2} \qquad (46)$$

where $\underline{\Omega}_0^{(0)}$ is the angular rotation vector for the off resonance Hamiltonian and $\underline{\Omega}_T^{(0)}$ is the angular rotation vector for the phase transient Hamiltonian. (The value of the phase transient was determined using the measured frequency at exact resonance, i.e. $\Delta\omega = 0$.) The small discrepency near the minimum point of the non-linear plot may be due to the higher order term,

$\bar{H}_{OT}^{(1)}$ the coupling term between the off resonance and the phase transient. Similar plots for the eight pulse cycle revealed linearity for several different values of J_1.

Finally we briefly explore the effects of second averaging (5,23). For the four pulse cycle, the non-zero dipolar coupling terms to the pulse imperfections will be at least partially removed by the second averaging process. As has been previously shown, second averaging about the offset axis for the four pulse cycle, averages $\bar{H}_D^{(2)}$ completely (5). For the eight pulse cycle, we see from Table II that the dipolar coupling terms to the pulse imperfections are all zero even before second averaging. As $\bar{H}_D^{(0)}$ and $\bar{H}_D^{(1)}$ are zero, the most important term controlling resolution is expected to be $\bar{H}_D^{(2)}$. Unfortunately, our calculations show that $\bar{H}_D^{(2)}$ is only partially removed by second averaging about the offset axis.

The phenomenon of second averaging had been previously discussed as an additional coherent averaging of the residual Hamiltonian about the rotation vector of the off resonance Hamiltonian (5,23). The theoretical analysis presented here shows that the second averaging axis will be modified by the existence of pulse errors. That is, the axis of second averaging will be generated by adding vectorially all those terms in Table II which are linearly dependent on the spin operators. Thus the present analysis shows how the effects of pulse errors on second averaging may be calculated without ambiguity.

REFERENCES

1. J. S. Waugh, L. M. Huber, and U. Haeberlen, Phys. Rev. Letters, 20, 180 (1968).

2. W. A. B. Evans, Ann. Phys., 48, 72 (1968).

3. J. S. Waugh, C. H. Wang, L. M. Huber, and R. L. Vold, J. Chem. Phys., 48, 662 (1968).

4. U. Haeberlen and J. S. Waugh, Phys. Rev., 175, 453 (1968).

5. U. Haeberlen, J. D. Ellett, Jr., and J. S. Waugh, J. Chem. Phys., 55, 53 (1971).

6. M. Mehring, R. G. Griffin, and J. S. Waugh, J. Am. Chem. Soc., 92, 7222 (1970).

7. L. M. Stacey, R. W. Vaughan, and D. D. Elleman, Phys. Rev. Letters, 26, 1153 (1971).

8. M. Mehring, R. G. Griffin, and J. S. Waugh, J. Chem. Phys., 55, 746 (1971).

9. R. W. Vaughan, D. D. Elleman, W-K Rhim, and L. M. Stacey, J. Chem. Phys., 57, 5383 (1972).

10. R. G. Griffin, J. D. Ellett, Jr., M. Mehring, J. C. Bullitt, and J. S. Waugh, J. Chem. Phys., 57, 2147 (1972).

11. J. D. Ellett, Jr., M. G. Gibby, U. Haeberlen, L. M. Huber, M. Mehring, A. Pines, and J. S. Waugh, Advances in Magnetic Resonance, (Ed. J. S. Waugh), Vol. 5, 117 (1971, Academic Press, New York.

12. R. W. Vaughan, D. D. Elleman, L. M. Stacey, W-K Rhim, and J. W. Lee, Rev. Sci. Instr., 43, 1356 (1972).

13. P. Mansfield, J. Phys. C 4, 1444 (1971).

14. P. Mansfield, M. J. Orchard, D. C. Stalker, and K. H. B. Richards, Phys. Rev. B 7, 90 (1973).

15a. W-K Rhim, D. D. Elleman, and R. W. Vaughan, J. Chem. Phys., 58, 1772 (1973).

15b. W-K Rhim, D. D. Elleman, and R. W. Vaughan, J. Chem. Phys., 59, 3740 (1973).

16. R. W. Vaughan, Annual Reviews in Materials Science, (Ed. by R. A. Huggins, R. H. Bube, R. W. Roberts), Vol. 4 (1974), Annual Reviews, Palo Alto.

17. M. Mehring and J. S. Waugh, Rev. Sci. Instr., 43, 649 (1972).

18. P. Mansfield, and U. Haeberlen, Z. Naturforsch, 28, 1081 (1973).

19. W. A. B. Evans and J. G. Powles, Proc. Phys. Soc. Longon, 92, 1046 (1967).

20. W. Magnus, Commun, Pure Appl. Math. 7, 649 (1954).

21. J. D. Ellett, Jr., and J. S. Waugh, J. Chem. Phys., 51, 2851 (1969).

22. This condition depends upon the equal spacing between the pulses in the flip-flop cycle. If the spacings between the pulses are not equal, the separation of phase errors and phase transient effects becomes more complicated, an iterative procedure being required (see Ref. 12).

23. A. Pines and J. S. Waugh, J. Mag. Res., 8, 354 (1972).

APPENDIX

The effects of power droop can not be studied in as general a fashion as other pulse errors, because the Hamiltonian is not periodic over time t_c. However, by assuming a specific model, that of exponential decay of the amplitude of the rf, one can compute the time development operator for the n'th cycle of the sequence, $U\left(nt_c \rightarrow (n+1)t_c\right)$ using the average Hamiltonian theory presented earlier. Thus the time development operator for the entire sequence $U\left(Nt_c\right)$ can be written,

$$U\left(Nt_c\right) = \prod_{n=0}^{N} U\left(nt_c \rightarrow (n+1)t_c\right)$$

where n increases from right to left.

Assuming exponential decay of $\omega_{rf}(t)$ from ω_1 to the steady-state value $\omega_1 - \omega_s$, one obtains for the droop errors, ω_d,

$$\omega_d(t) = \omega_{rf}(t) - \omega_1 = -\omega_s\left(1 - e^{-t/b\tau}\right) \tag{A-1}$$

where the time τ is indicated in Fig. 1 and b is a dimensionless time constant. It is assumed $b >> 1$ and that droop during the width of the pulse may be neglected.

The average Hamiltonians over the n'th cycle for the four pulse and eight pulse cycles are presented in Table II. Since $\bar{H}_d^{(0)}$ changes during the sequence, the effective rotation vector will change during the sequence. Thus, the observed frequency of the signal may have one value at the start of the sequence and a different value later in the pulse chain, thus distorting the spectra obtained.

In order to estimate the size of this frequency modulation effect for the four pulse sequence, parameters were chosen to be $t_c = 25$ μsec, $\omega_s t_w = \pi/40$, and $b = 100$. Using the results from Table II , one obtains

$$\frac{\omega_s t_w}{t_c} \frac{2}{b} \approx 63 \text{ rad/sec}$$

Thus, the frequency modulation effect could be important for the four pulse sequence.

On the other hand, for the eight pulse sequence an additional factor of 1/b appears in $\bar{H}_d^{(0)}$, thus reducing its importance. For t_c = 50 μsec, $\omega_s t_w = \pi/40$, and b = 100, one obtains

$$\frac{\omega_s t_w}{t_c} \frac{12}{b^2} \approx 2 \text{ rad/sec}$$

Thus, frequency modulation is not expected to be as great a problem for the eight pulse sequence as for the four pulse sequence.

The power droop error can also couple with the dipolar Hamiltonian. Since the error produced by power droop changes during the sequence, not only can this term, $\bar{H}_{dD}^{(1)}$ (n'th cycle), diminish resolution, but it also can severely distrot the form of the lineshape. From the results in Table II, one expects this effect to be much smaller for the eight pulse cycle than for the four pulse cycle. This is understandable since the four pulse cycle is very sensitive to overall pulse width errors, whereas the eight pulse cycle is not (15b).

Experimentally, confirmation of $\bar{H}_{dD}^{(1)}$ for the four pulse cycle is difficult since, as was previously reported (15b), the signal occurring from decay to decay was found to fluctuate. Such fluctuations did not occur for the eight pulse cycle and the lineshape for the CaF_2 crystal, with the (111) crystallographic axis parallel to the external field was found to be Lorentzian. As has been shown, power droop and other pulse errors are not expected to couple strongly with the dipolar Hamiltonian for the eight pulse cycle. Thus one may be able to compare profitably theoretical lineshapes with experimental lineshapes.

TABLE I

Average Hamiltonians and their Correction Terms for Tuneup Cycles

(0 - Offset, P - Phase Error)	T - Phase Transient, δ - Pulse Width Error	ε - rf Inhomogeneity, d - Power Droop
	$\left(\frac{\pi}{2}\right)_x - \left(\frac{\pi}{2}\right)_x - \left(\frac{\pi}{2}\right)_x - \left(\frac{\pi}{2}\right)_x$	Flip-Flop Cycle
$\bar{H}_0^{(0)a}$	0	$\frac{\Delta\omega}{2}\left(1 + \frac{2}{3}a\right)\left(I_z - I_y\right)$
$\bar{H}_0^{(1)}$	$-\frac{t_c}{16}\left(\Delta\omega\right)^2 I_x$	0
$\bar{H}_P^{(0)}$	0	$\frac{1}{t_c}\left(-\phi_x + \phi_{-x}\right)\left(I_y + I_z\right)$
$\bar{H}_{P0}^{(1)}$	0	$\frac{\Delta\omega}{4}\left(\phi_x + \phi_{-x}\right)I_x$
$\bar{H}_T^{(0)b}$	0	$\frac{1}{t_c} J_1\left(I_z - I_y\right)$
$\bar{H}_{T0}^{(1)}$	$-\frac{\Delta\omega}{2} J_1 I_x$	$-\frac{\Delta\omega}{4} J_2 I_x$
$\bar{H}_\delta^{(0)}$	$-\frac{4}{t_c}\delta_x I_x$	$\frac{1}{t_c}\left(-\delta_x + \delta_{-x}\right)I_x$
$\bar{H}_{\delta 0}^{(1)}$	$\frac{\Delta\omega}{2}\delta_x I_z$	$-\frac{\Delta\omega}{4}\left(\delta_x + \delta_{-x}\right)I_z$
$\bar{H}_\varepsilon^{(0)}$	$-\frac{4}{t_c}\sum_i \varepsilon_i I_{xi}$	0
$\bar{H}_{\varepsilon 0}^{(1)}$	$\frac{\Delta\omega}{2}\sum_i \varepsilon_i I_{zi}$	$-\frac{\Delta\omega}{2}\sum_i \varepsilon_i I_{zi}$

TABLE I (continued)

	$\left(\frac{\pi}{2}\right)_x - \left(\frac{\pi}{2}\right)_x - \left(\frac{\pi}{2}\right)_x - \left(\frac{\pi}{2}\right)_x$	Flip-Flop Cycle
$\tilde{H}_d^{(0)}$ $\left(\text{n'th cycle}\right)^c$	$-\frac{\omega_s t_w}{t_c} 4\left(1 - e^{-8n/b}\right) I_x$	$\frac{\omega_s t_w}{t_c} \frac{2}{b} e^{-4n/b} I_x$

a $\quad a = \frac{3t_w}{t_c}\left(\frac{4}{\pi} - 1\right)$

b $\quad J_1 = \int_0^{t_w} \omega_T(t)\left(\sin \omega_1 t - \cos \omega_1 t\right) dt$

$\quad J_2 = \int_0^{t_w} \omega_T(t)\left(\sin \omega_1 t + \cos \omega_1 t\right) dt$

c $\quad \tilde{H}_d^{(0)}(\text{n'th cycle}) = \tilde{H}_d^{(0)}\left(nt_c \rightarrow (n+1)t_c\right)$. Exponential decay of $\omega_{rf}(t)$ with time constant $b\tau$; $b >> 1$ is assumed.

TABLE II

Average Hamiltonians and their Correction Terms for the Four Pulse and Eight Pulse Cycles.

(0 - Offset; D - Dipolar; P - Phase Error; T - Phase Transient; δ - Pulse Width Error; ε - rf Inhomogeneity; d - Power Droop)

	Four Pulse (WHH) Cycle	Eight Pulse Cycle
$\bar{H}_0^{(0)}$[a]	$\frac{1}{3}\sum_i\left(\Delta\omega + \omega_o\sigma_{zzi}\right)(1+a)\left(I_{xi} + I_{yi} + I_{zi}\right)$	$\frac{1}{3}\sum_i\left(\Delta\omega + \omega_o\sigma_{zzi}\right)(1+2a)\left(I_{xi} + I_{zi}\right)$
$\bar{H}_0^{(1)}$	0	$\frac{t_c}{36}\sum_i\left(\Delta\omega + \omega_o\sigma_{zzi}\right)^2\left(I_{xi} - I_{zi}\right)$
$\bar{H}_D^{(0)}$	$-\sum_{i<j}B_{ij}\frac{6}{\pi}\frac{t_w}{t_c}\left[I_{yi}\left(I_{xj} + I_{zj}\right) + \left(I_{xi} + I_{zi}\right)I_{yj}\right]$	0
$\bar{H}_D^{(1)}$	0	0[b]
$\bar{H}_D^{(2)}$	$\frac{t_c^2}{648}\left[H_D^{(x)} - H_D^{(z)}, \left[H_D^{(x)}, H_D^{(y)}\right]\right]$	$\frac{t_c^2}{2592}\left[H_D^{(x)} - H_D^{(z)}, \left[H_D^{(x)}, H_D^{(y)}\right]\right]$
$\bar{H}_{DO}^{(1)}$	0	0
$\bar{H}_{DO}^{(2)}$[c]	d	$\frac{t_c^2}{864}(\Delta\omega)\left[I_x, \left[H_D^{(x)}, H_D^{(y)}\right]\right] + \frac{t_c^2}{432}\left(\Delta\omega\right)^2\left(H_D^{(z)} - H_D^{(x)}\right)$

TABLE II (continued)

	Four Pulse (WHH) Cycle	Eight Pulse Cycle
$\bar{H}_P^{(0)}$	$\frac{1}{t_c}\left[\left(\phi_y - \phi_{-y}\right)I_x + \left(-\phi_x + \phi_{-x} - \phi_y + \phi_{-y}\right)I_y + \left(\phi_x - \phi_{-x}\right)I_z\right]$	$\frac{2}{t_c}\left[\left(\phi_y - \phi_{-y}\right)I_x + \left(-\phi_x + \phi_{-x}\right)I_y\right]$
$\bar{H}_{PO}^{(1)}$	$\frac{1}{6}\sum_i\left(\Delta\omega + \omega_o\sigma_{zzi}\right)\left[-\left(\phi_x + \phi_{-x}\right)\left(I_{xi} - I_{yi}\right) + \left(\phi_x + \phi_{-x} - \phi_y - \phi_{-y}\right)I_{zi}\right]$	$\frac{1}{6}\sum_i\left(\Delta\omega + \omega_o\sigma_{zzi}\right)\left[\left(-\phi_y + \phi_{-y}\right)I_{xi} + 2\phi_x I_{yi}\right]$
$\bar{H}_{PD}^{(1)}$	$\frac{1}{2}\left(-\phi_x - \phi_{-x} + \phi_y + \phi_{-y}\right)\sum_{i<j}B_{ij}\left(I_{xi}I_{zj} + I_{zi}I_{xj}\right)$	0
$\bar{H}_T^{(0)g}$	$\frac{1}{t_c}J_1\left(I_x + 2I_y + I_z\right)$	$\frac{2}{t_c}J_1\left(I_x + I_z\right)$
$\bar{H}_{TO}^{(1)g}$	$\frac{1}{6}J_2\sum_i\left(\Delta\omega + \omega_o\sigma_{zzi}\right)\left(I_{xi} - I_{yi}\right)$	$\frac{1}{6}\sum_i\left(\Delta\omega + \omega_o\sigma_{zzi}\right)\left[3J_1\left(I_{xi} - I_{zi}\right) - J_2 I_{yi}\right]$
$\bar{H}_{TD}^{(1)}$	0	0
$\bar{H}_\delta^{(0)}$	$\frac{1}{t_c}\left[\left(-\delta_x + \delta_{-x}\right)I_x + \left(\delta_y - \delta_{-y}\right)I_z\right]$	$\frac{2}{t_c}\left(-\delta_x + \delta_{-x}\right)I_x$
$\bar{H}_{\delta O}^{(1)}$	$-\frac{1}{6}\sum_i\left(\Delta\omega + \omega_o\sigma_{zzi}\right)\left[\left(\delta_x + \delta_{-x}\right)I_{zi} + \left(\delta_y + \delta_{-y}\right)I_{yi}\right]$	$\frac{1}{6}\sum_i\left(\Delta\omega + \omega_o\sigma_{zzi}\right)\left[-2\delta_{-x}I_{zi} + \left(\delta_y - \delta_{-y}\right)I_{yi}\right]$
$\bar{H}_{\delta D}^{(1)}$	$\frac{1}{2}\sum_{i<j}B_{ij}\left[\left(\delta_x + \delta_{-x}\right)\left(I_{yi}I_{zj} + I_{zi}I_{yj}\right) + \left(\delta_y + \delta_{-y}\right)\left(I_{xi}I_{yj} + I_{yi}I_{xj}\right)\right]$	0

TABLE II (continued)

	Four Pulse (WHH) Cycle	Eight Pulse Cycle
$\bar{H}_{\epsilon}^{(0)}$	0	0
$\bar{H}_{\epsilon 0}^{(1)}$	$-\frac{1}{3}\sum_i \epsilon_i \left(\Delta\omega + \omega_o \sigma_{zzi}\right)\left(I_{yi} + I_{zi}\right)$	$-\frac{1}{3}\sum_i \epsilon_i \left(\Delta\omega + \omega_o \sigma_{zzi}\right) I_{zi}$
$\bar{H}_{\epsilon D}^{(1)e}$	$\sum_{i<j}\sum \epsilon_i B_{ij}\left[I_{yi}\left(I_{xj} + I_{zj}\right) + \left(I_{xi} + I_{zi}\right) I_{yj}\right]$	0
$\bar{H}_{d}^{(0)}$ (n'th cycle)	$-\frac{\omega_s t_w}{t_c}\frac{2}{b} e^{-6n/b}\left(2I_x + I_z\right)$	$\frac{\omega_s t_w}{t_c}\frac{12}{b^2} e^{-12n/b}\left(2I_x + I_z\right)$
$\bar{H}_{dD}^{(1)}$ (n'th cycle)	$\omega_s t_w\left[1 + \left(-1 + \frac{3}{b}\right)\exp(-6n/b)\right]$ $x\sum_{i<j}\sum B_{ij}\left[I_{yi}\left(I_{xj} + I_{zj}\right) + \left(I_{xi} + I_{zi}\right) I_{yj}\right]$	$\frac{3\omega_s t_w}{b}\exp(-12n/b)\sum_{i<j}\sum B_{ij}\left[I_{yi}\left(I_{xj} + I_{zj}\right) + \left(I_{xi} + I_{zi}\right) I_{yj}\right]$

a $a = \frac{3t_w}{t_c}\left(\frac{4}{\pi} - 1\right)$

b For the eight pulse cycle, even for pulses of finite width, $\bar{H}_D^{(1)} = 0$.

c This calculation assumes all nuclei are chemically and geometrically equivalent.

d $$\bar{H}_{D0}^{(2)} = \frac{t_c^2}{648}\Big\{-3\Delta\omega\left[H_D^{(x)},\left[H_D^{(y)},I_x\right]\right] - 3\Delta\omega\left[H_D^{(z)},\left[H_D^{(x)},I_y\right]\right] + \left(\Delta\omega\right)^2\left[I_y + I_z,\left[H_D^{(y)},I_x\right]\right]$$
$$+ \left(\Delta\omega\right)^2\left[4I_x + 3I_y + I_z,\left[H_D^{(x)},I_y\right]\right] + i\left(\Delta\omega\right)^2\left[H_D^{(y)},I_x\right] - i\left(\Delta\omega\right)^2\left[H_D^{(x)},I_y\right] + i\left(\Delta\omega\right)^2\left[H_D^{(x)},I_z\right]\Big\}$$

TABLE II (continued)

e It is assumed that ω_1 is constant over a scale of molecular dimensions.

f $\bar{H}_d^{(0)}(\text{n'th cycle}) = \bar{H}_d^{(0)}\left(nt_c \rightarrow (n+1)t_c\right)$ and similarly for $\bar{H}_{dD}^{(1)}$.

Exponential decay of $\omega_{rf}(t)$ with time constant $b\tau$; $b \gg 1$ is assumed.

g $$J_1 = \int_o^{t_w} \omega_T(t)\left(\sin \omega_1 t - \cos \omega_1 t\right)dt$$

$$J_2 = \int_o^{t_w} \omega_T(t)\left(\sin \omega_1 t + \cos \omega_1 t\right)dt$$

FIGURE CAPTIONS

Figure 1. Ideal pulse cycles. All pulses are $\pi/2$ with phases as indicated. (a) flip-flop cycle, (b) $90_x - 90_x - 90_x - 90_x$ cycle, (c) four pulse cycle, (d) eight pulse cycle.

Figure 2. Effects of pulse errors on the flip-flop cycle ($t_c = 61.25$ μsec). The horizontal scale is 2 msec per division. (a) Well tuned spectrometer at resonance. Slight decay of upper trace is due to inhomogeneity of static magnetic field. (b) Same as (a) but with offset frequency of 1 KHz. (c) Same as (a) but with phase error in x pulses of 5°. (d) Same as (a) but with pulse width of x pulses decreased about 5.8°. (e) Same as (a) but with phase transient changed.

Figure 3. Chemical shift scaling curves for the $90_x - 90_x - 90_x - 90_x$ cycle ($t_c \sim 260$ μsec). Circles are experimental points obtained with phase transient effect eliminated, $J_1 = 0$. Triangles are experimental points obtained with $J_1 < 0$. Solid curves are obtained from Eq. (44).

Figure 4. Effect of phase transients on $90_x - 90_x - 90_x - 90_x$ cycle. Plotted on the abscissa is the observed frequency from the flip-flop cycle ($t_c \sim 30$ μsec). Plotted along the ordinate is the slope at resonance of the chemical shift scaling curve for the $90_x - 90_x - 90_x - 90_x$ cycle. Refer to Equation (45).

Figure 5. Chemical shift scaling curves for the four pulse cycle. Circles are experimental points obtained with phase transient effect nearly eliminated. Triangles are experimental points obtained with $J_1 < 0$. Solid curves are obtained from Equation (46).

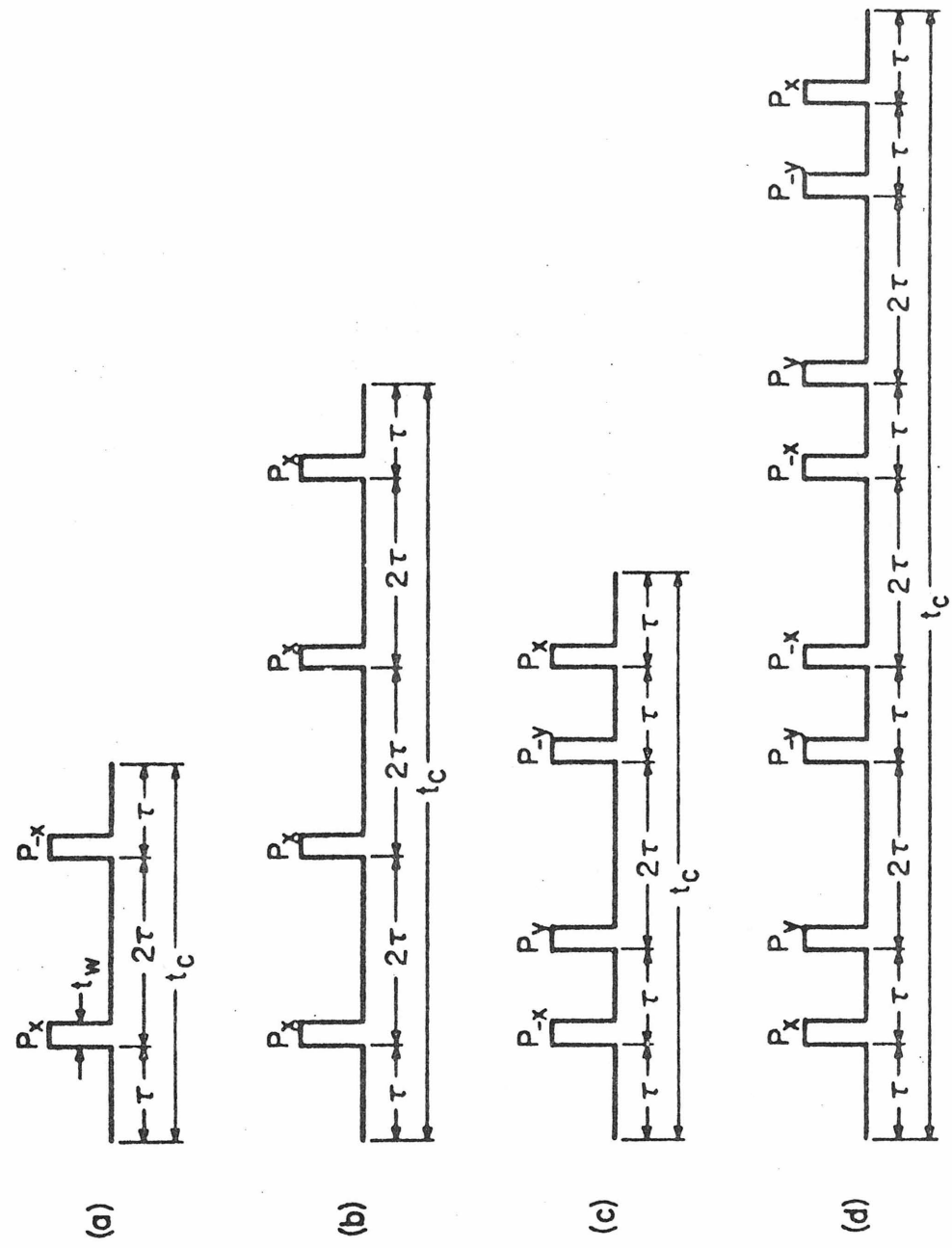

FIGURE
1

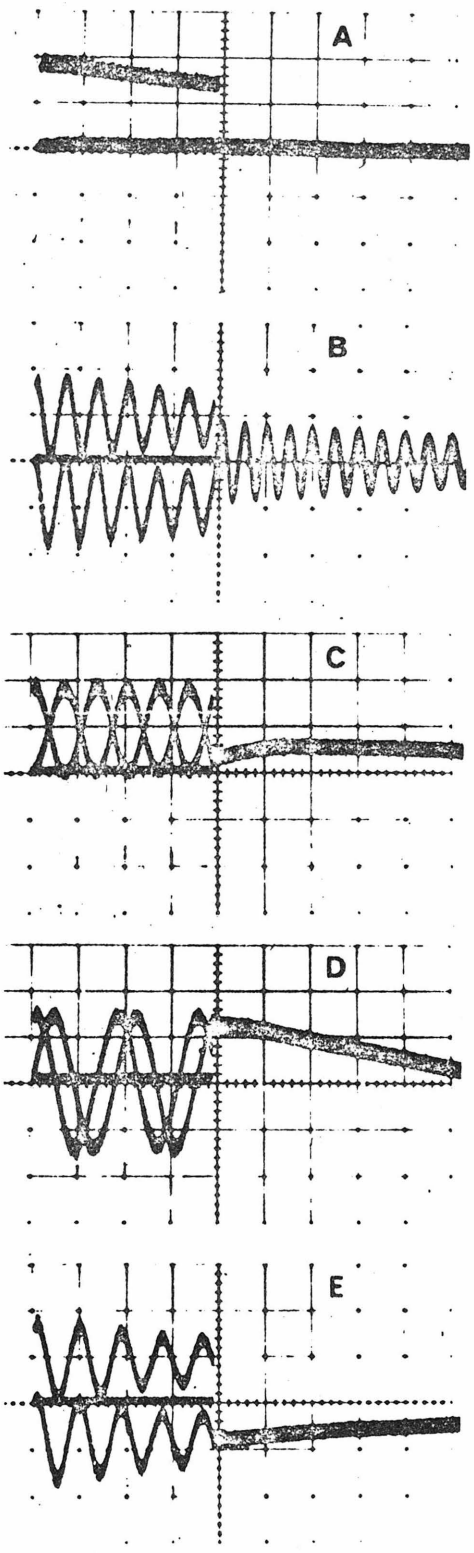

FIGURE
2

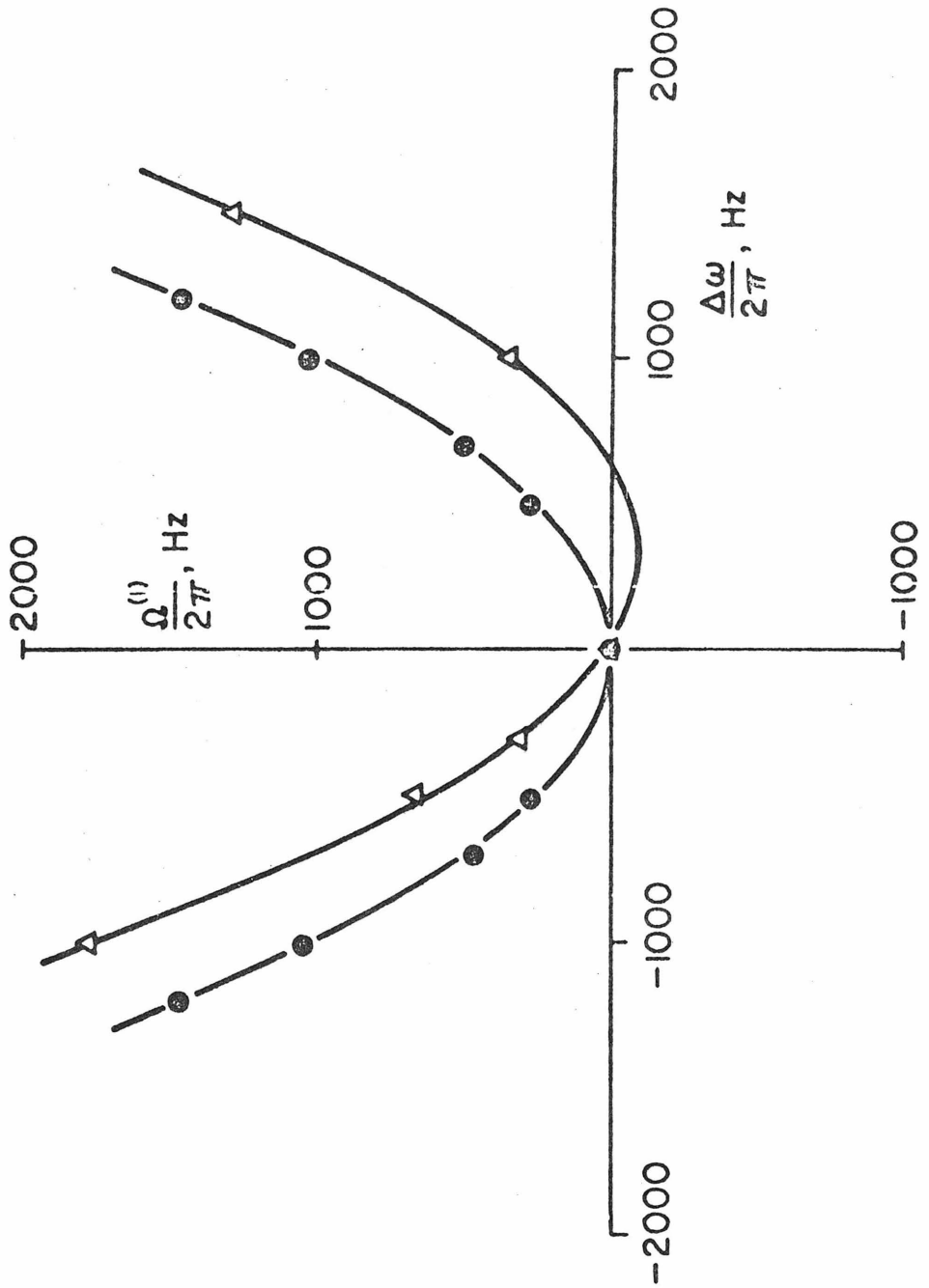
2000
1000
-1000
-2000
$\frac{\Omega^{(1)}}{2\pi}$, Hz
2000
1000
-1000
-2000
$\frac{\Delta\omega}{2\pi}$, Hz

FIGURE
3

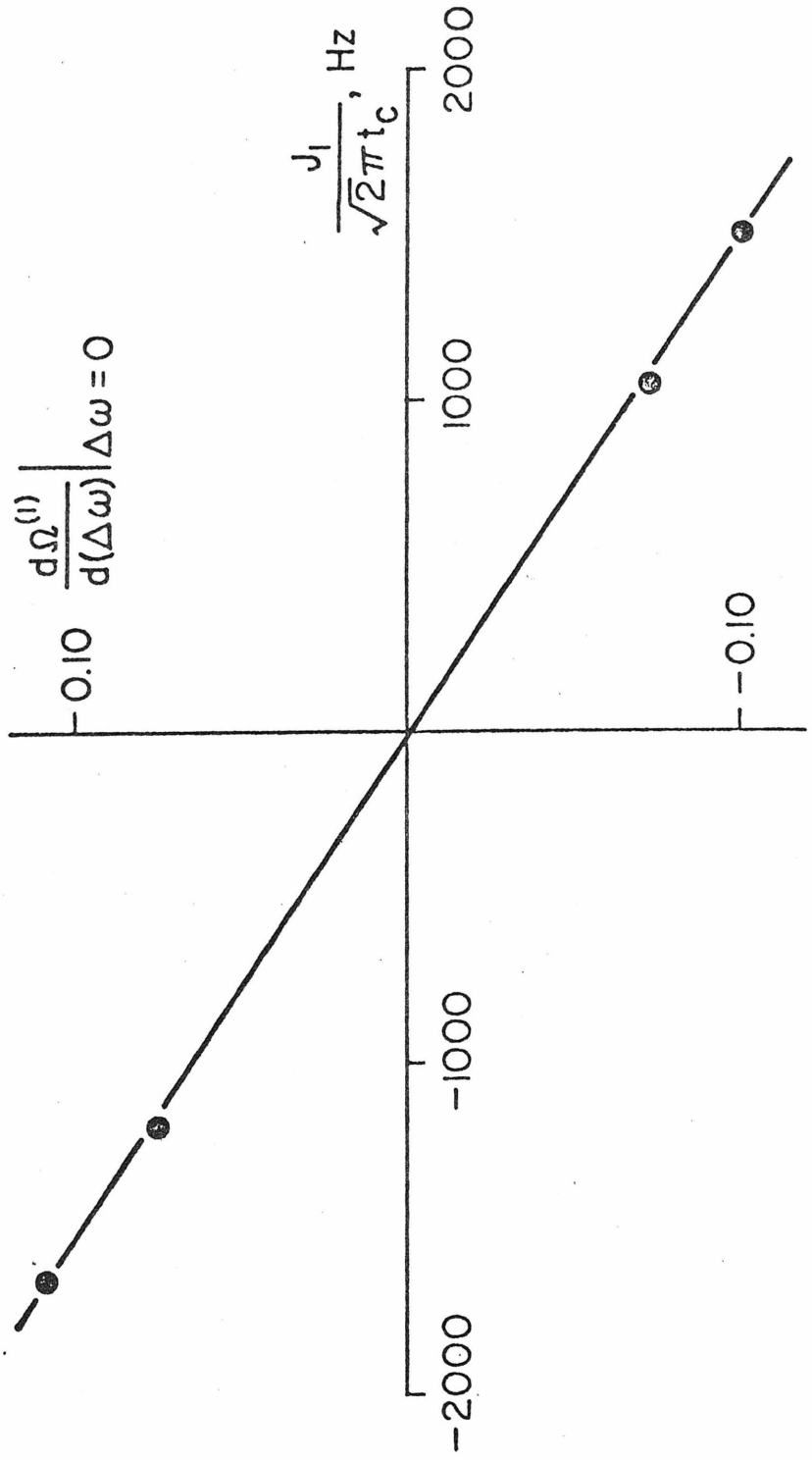
$\frac{d\Omega^{(1)}}{d(\Delta\omega)}\Big|_{\Delta\omega=0}$
0.10
−0.10
$\frac{J_1}{\sqrt{2}\pi t_c}$, Hz
2000
1000
−1000
−2000

FIGURE
4

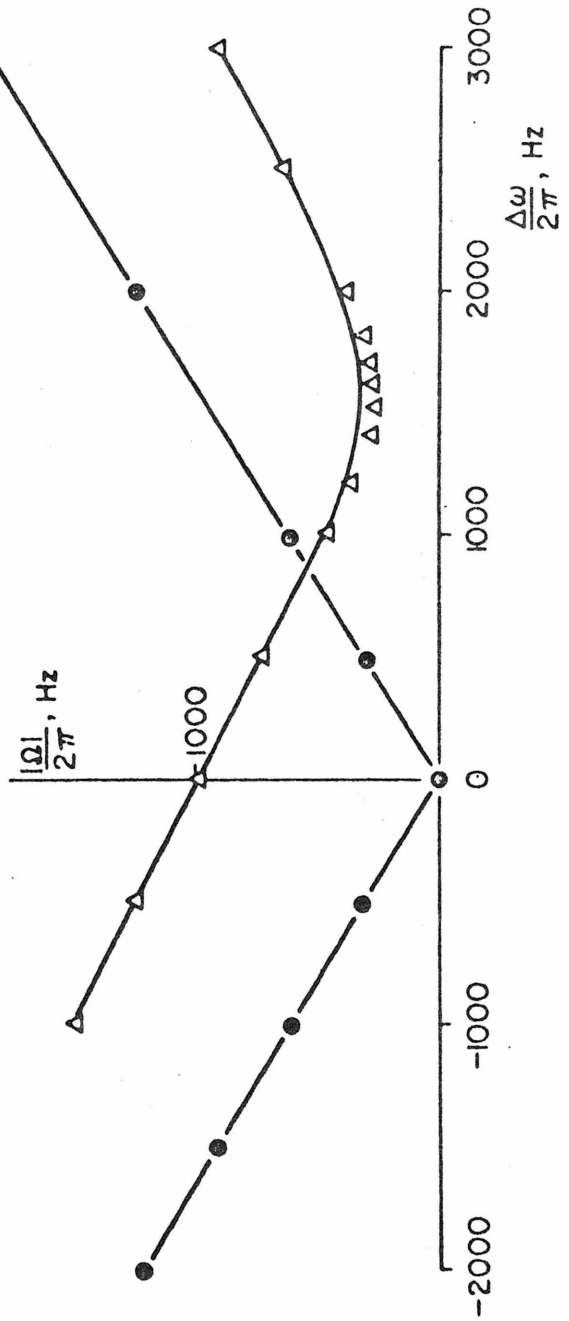
$\frac{|\Omega|}{2\pi}$, Hz
1000
0
-1000
-2000
1000
2000
3000
$\frac{\Delta\omega}{2\pi}$, Hz

FIGURE
5

CHAPTER 3

THE CHEMICAL SHIFT TENSOR FOR THE HYDROXYL PROTON: $Ca(OH)_2$

(The text of Chapter 3 consists of an article coauthored with R. W. Vaughan that has appeared in Chemical Physics Letters, Vol. 28, No. 4, 15 October 1974.)

The development of multiple pulse techniques for high resolution NMR in solids (1-10) has made it possible to directly measure the proton chemical shift tensor for the first time and, within recent months, reports of initial studies have begun to appear (4,11-17). These have involved numerous investigations of carboxylic groups (4,11-12,14-17), one study of a water molecule (13), and a partial characterization of protons in other compounds (11,15,17). Studies of protons in carboxylic groups and in the water molecule of $MgSO_4.H_2O$ involve examining a proton in a near linear hydrogen bonded arrangement, -O-H····O-. It is the purpose of this letter to present the proton chemical shift tensor for the non-hydrogen bonded case, i.e. the hydroxyl group, $-O-H^-$. Measurements were made in a single crystal of $Ca(OH)_2$ as this material furnishes a particularly attractive model system in which the non-hydrogen bonded nature of the hydroxyl group is well characterized (18-19). All protons within this material are in equivalent positions and the point symmetry of the proton sites is sufficiently high (20) to require the proton chemical shift tensor to be axially symmetric with its symmetry axis parallel to the 001 crystallographic axis. Thus two measurements, one parallel and one perpendicular to the 001 crystallographic axis, will completely determine the proton chemical shift tensor.

Measurements were made using a previously introduced eight pulse cycle (4) with a cycle time of 36 μsec and a spectrometer previously described (4,21). The crystal was grown and kindly furnished by Professor F. Holuj of the University of Windsor and consisted of a rough parallelepiped 5mm x 5mm x 3mm. Because the interproton distances are very short in this material, the ratio of the experimental cycle time, t_c, to the dipolar

decay constant, T_2, could not be made small enough to allow one to ignore the higher order correction terms to the average Hamiltonian (2). One observes, therefore, rather large linewidths which are a function of crystal orientation (as T_2 is a function of orientation). This is illustrated in Figure 1 where the two spectra needed to determine the proton chemical shift tensor are reproduced. Since the crystal cleaved easily along the 001 plane, this cleavage surface was used as a reference to initially orient the crystal. Rotation spectra were taken about an axis lying within 2° of the 001 plane at 5° intervals and exhibited the expected behavior of an axially symmetric tensor with its symmetry axis perpendicular to the 001 plane. Two spectra corresponding to the extremes of the rotation pattern (and which were orientated parallel and perpendicular to the 001 plane) are reproduced in Figure 1. The observed spectra furnish values of $\sigma_{\parallel} = 3.5 \pm 1$ ppm and $\sigma_{\perp} = -8.7 \pm 1$ ppm and indicate a chemical shift anisotropy $(\sigma_{\parallel} - \sigma_{\perp})$ of 12.2 ± 1 ppm.

As the $Ca(OH)_2$ crystal cleaves easily it was not possible to shape the sample into a spherical shape and it is necessary to correct the values obtained from the spectra in Figure 1 for bulk susceptibility effects. By approximating the crystal as an ellipsoid (b/a = 1.0, c/a = 0.6 with a, b, c the semi-axes) and using the tabulated results of Osborn (22) together with a value of -0.665×10^{-6} for the volume susceptibility of $Ca(OH)_2$ (23), one estimates correction factors of - 0.6 ppm for $\sigma_{\perp}$ and 1.2 ppm for $\sigma_{\parallel}$. If these are applied to the spectra in Figure 1, one finds that $\sigma_{\perp} = -9.3 \pm 1$ ppm and $\sigma_{\parallel} = +4.7 \pm 1$ ppm relative to a spherical sample of TMS. An anisotropy, $\sigma_{\parallel} - \sigma_{\perp}$, of 14 ± 1 ppm thus exists in the proton chemical shift tensor for the hydroxyl proton in $Ca(OH)_2$. This can be

compared to anisotropies of 18-26 ppm reported for hydrogen bonded protons (4,11-12,14-17). The trace of the hydroxyl proton tensor is - 4.6 ppm relative to TMS and this is more positive than the hydrogen bonded protons by several ppm. However, it is not possible to be more precise on this point as previous authors have ignored the susceptibility correction terms. Even if the samples have ellipsoidal shapes, the omission of detailed shape of both the main and reference samples produces several ppm ambiguity in the reported results, as it is not possible for the reader to make the necessary susceptibility corrections.

REFERENCES

1. R. W. Vaughan, Annual Reviews in Materials Science, (Ed. by R. A. Huggins, R. H. Bube, R. W. Roberts), Vol. 4 (1974), Annual Reviews, Palo Alto, and references therein.

2. J. S. Waugh, L. M. Huber, and U. Haeberlen, Phys. Rev. Letters, 20, 180 (1968); U. Haeberlen and J. S. Waugh, Phys. Rev., 175, 453 (1968).

3. P. Mansfield, J. Phys. C 4, 1444 (1971).

4. W-K. Rhim, D. D. Elleman, and R. W. Vaughan, J. Chem. Phys., 58, 1772 (1973); 59, 3740 (1973).

5. W-K. Rhim, D. D. Elleman, L. B. Schreiber and R. W. Vaughan, scheduled for J. Chem. Phys., June 2, 1974 issue.

6. M. Mehring, R. G. Griffin, and J. S. Waugh, J. Am. Chem. Soc., 92, 7222 (1970).

7. L. M. Stacey, R. W. Vaughan, and D. D. Elleman, Phys. Rev. Letters, 26, 1153 (1971).

8. M. Mehring, R. G. Griffin, and J. S. Waugh, J. Chem. Phys., 55, 746 (1971).

9. R. G. Griffin, J. D. Ellett, Jr., M. Mehring, J. C. Bullitt, and J. S. Waugh, J. Chem. Phys., 57, 2147 (1972).

10. R. W. Vaughan, D. D. Elleman, W-K. Rhim, and L. M. Stacey, J. Chem. Phys., 57, 5383 (1972).

11. U. Haeberlen, Proceedings of the 1st Specialized Colloque Ampere, Krakow, Poland (1973) page 28.

12. R. W. Vaughan, W-K. Rhim, and D. D. Elleman, Proceedings of the 1st Specialized Colloque Ampere, Krakow, Poland (1973) page 129.

13. U. Haubenreisser and B. Schnabel, Proceedings of the 1st Specialized Colloque Ampere, Krakow, Poland (1973) page 140.

14. P. Van Hecke, J. C. Weaver, B. L. Neff and J. S. Waugh, Proceedings of the 1st Specialized Colloque Ampere, Krakow, Poland (1973) page 143; J. Chem. Phys., 60, 1668 (1974).

15. U. Haeberlen and U. Kohlschutter, Chem. Phys. 2, 76 (1973).

16. H. Raber, G. Brunger and M. Mehring, Chem. Phys. Letters, 23, 400 (1973).

17. U. Haeberlen, U. Kohnschutter, J. Kempt, H. W. Spiess and H. Zimmermann, Chem. Phys., 3, 248 (1974).

18. J. D. Bernal and H. D. Megaw, Proc. Roy. Soc. A 151, 384 (1935)

19. H. E. Petch, Acta. Cryst., 14, 950 (1961).

20. A. D. Buckingham and S. M. Malin, Mole. Phys. 22, 1127 (1971).

21. R. W. Vaughan, D. D. Elleman, L. M. Stacey, W-K. Rhim and J. W. Lee, Rev. Sci. Instr., 43, 1356 (1972).

22. J. A. Osborn, Phys. Rev., 67, 351 (1945).

23. 47th Edition of the Chemical Rubber Handbook, Chemical Rubber Publishing Co., Cleveland, Ohio.

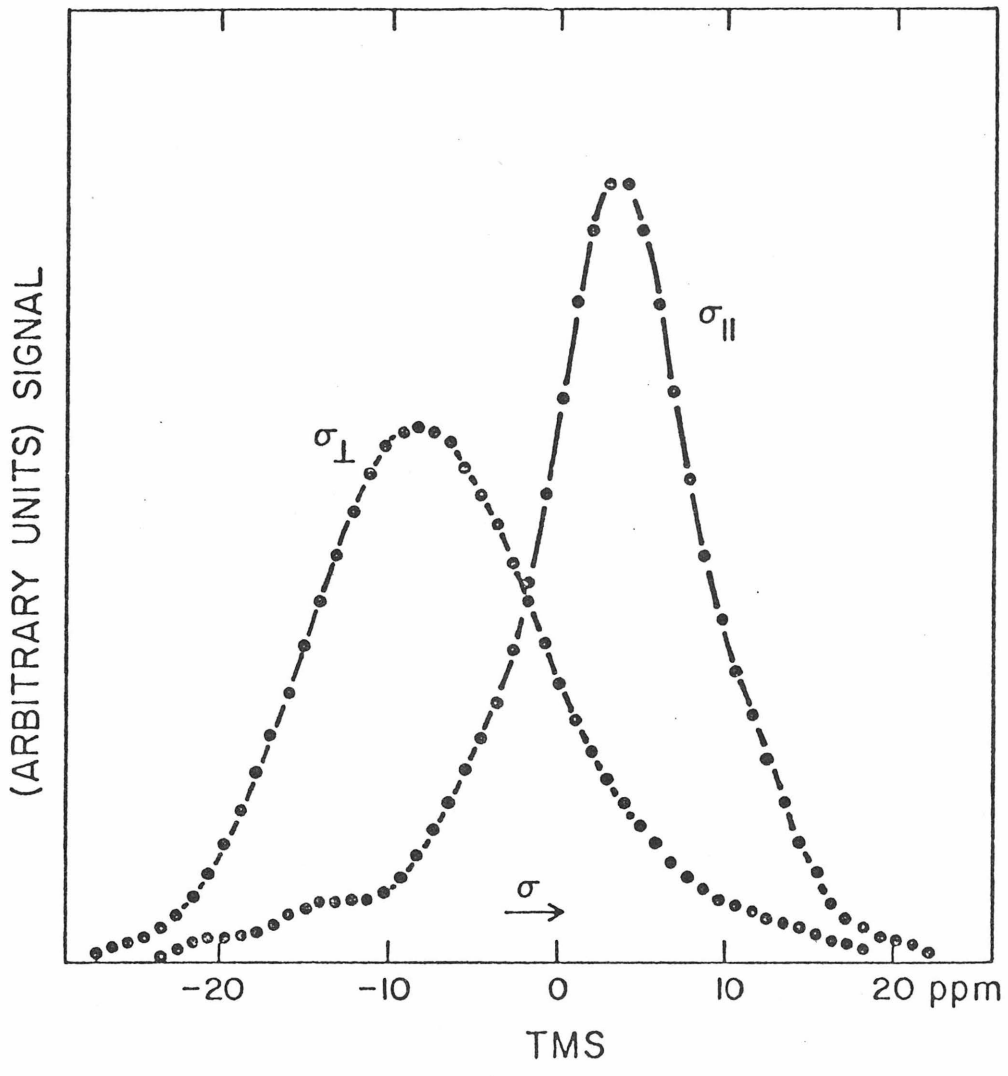

Figure 1 Single crystal spectra of $Ca(OH)_2$ taken with the crystal 001 axis (and consequently the OH^- direction) both parallel and perpendicular to the magnetic field direction.

CHAPTER 4

A NMR INVESTIGATION OF HIGH SURFACE AREA SILICA-ALUMINAS

(The text of Chapter 4 consists of an article coauthored with R. W. Vaughan that has been accepted for publication in Journal of Catalysis.)

INTRODUCTION:

This paper presents results of a nuclear magnetic resonance (NMR) study of hydroxyl protons bound to the surface of silica-aluminas whose composition varied from 0 - 100% SiO_2. The surface hydroxyl groups on high surface area silica have been extensively studied, particularly by infrared (1,2) and NMR techniques (3-8). Some NMR studies have been reported of hydroxyl groups on an 87.5% silica-12.5% alumina sample (5,9,10) and on pure alumina (11, 12). However, the present work represents to the authors' knowledge the only attempt using NMR to examine surface hydroxyls on a whole series of silica-aluminas. In addition, a variety of "multiple-pulse" NMR techniques has been used in this work in addition to conventional pulsed NMR, and thus some of the difficulties associated with the interpretation of NMR results for surface species have been avoided.

EXPERIMENTAL DETAILS:

Sample Preparation. The samples used in this work were prepared by Dr. D. A. Hickson at the Chevron Laboratories in Richmond, California, and have been the subject of a publication by James A. Schwarz (13) where selective adsorption coupled with infrared techniques was used to characterize the nature of the acid sites on the surfaces. The samples were prepared by mixing desired amounts of $AlCl_3$ and tetraethyl ortho silicate in methanolic solution (14). The resulting solution was homogeneously gelled by the addition of propylene oxide, thus raising the pH. The methanol was then displaced by rinsing in diethyl ether. The material was then placed in an autoclave, and the temperature was brought to the critical point for diethyl

ether. The vapor was flushed away with dry nitrogen. This resulted in an extremely high surface area material. Infrared techniques were used to demonstrate that hydroxyl groups in these materials rapidly exchanged with D_2O vapor and thus represent surface groups (15).

Sample Pretreatment. A cavity for containment of each sample was formed from a 15-cm length of 4-mm quartz tubing by blowing out the bottom 10 mm of the tube to 5 mm o.d. and then sealing that end. This procedure produced a cavity with an i.d. of 4-1/2 mm which was packed with the sample, containing typically 20-40 mg of material with a surface area of 12 to 24 square meters. The open end of each tube was attached to a glass vacuum system of two-liter volume for treatment of the samples. The vacuum system was greaseless and produced a pressure of 10^{-7} torr. Two samples of each composition were prepared. The first sample was calcined in 152 torr of oxygen for one hour at 500^{o} C and then sealed. The second sample, after being calcined for one hour at 500^{o} C, was cooled to 150^{o} C and exposed to water vapor at 4.6 torr for one hour, evacuated, and then sealed.

NMR Apparatus. The NMR measurements were conducted at room temperature and at 56.4 MHz. Signal averaging was used (256 decays) and an external deuterium lock system held the magnet field drift to a few milligauss during the period of several hours normally needed for signal averaging (T_1's were all in the 20-second range). Free induction decay spectra were taken well off resonance (50 KHz) and the envelope of the observed oscillation used to determine the decay. This technique involves giving up a substantial portion of the available signal to noise and accounts for much of the experimental scatter observed in Figures 1 to 5. However, it assures that the reported

decays are not contaminated by artifacts.

The basic multiple pulse NMR spectrometer has been previously described (16). The sample coil was constructed as earlier reported to minimize rf inhomogeneity (17), and the quality factor, Q, of the probe was 40. It was found necessary to use components constructed with teflon dielectric for items in and near the probe to eliminate anomalous proton signals.

The presence of any small transients due to pulse overload of the receiving circuits can mask the low-level signals available from these measurements. Thus, several pulse buffers were installed which improved the receiver overload characteristics. Each pulse buffer was a passive circuit consisting of a Relcom BT9 transformer (18) to increase impedence of the signal to 800 ohms, three sets of crossed diodes (germanium 1N270) across the 800 ohms (for clipping the rf pulse), and a second Relcom BT9 to transform the signal back to 50 ohms. Such buffers limited pulses of several volts at the input to ∿70 mv rms at the output with an attenuation of the low level signals of 6 db. In addition to using such a buffer before the receiver, it was found advantageous to place a buffer between several of the Avantek unit amplifiers (19) used in the receiver. Apparently this allowed one to minimize the poorly understood nonlinear overload characteristics of these particular unit amplifiers. Under these conditions the small signals from these experiments could be characterized approximately four microseconds after the end of the rf pulse.

The data acquisition system consisted of a Biomation 802 Transient recorder interfaced to a PDP8/e computer equipped with a PDP TU60 tape cassette data storage system.

NMR Techniques. The application of NMR techniques has furnished

information on the (a) number, (b) arrangement, (c) bonding, and (d) motion of hydroxyl groups on the materials studied.

(a) The number, or density, of hydroxyls on the materials was determined from the initial magnitude of the free induction decay observed after a 90^{o} pulse. Care has to be taken that the sample is at equilibrium with the magnetic field before application of the 90^{o} pulse. The magnitude of the free induction decay was calibrated by using samples of known proton content.

(b) Information on the local environment and arrangement of hydroxyl groups on the surface was obtained from an analysis of the free induction decay lineshape, either directly or by use of a moment analysis (20).

(c) Information on the chemical bonding of the hydroxyl groups to these materials has been obtained by using the multiple pulse NMR techniques (21) to measure components of the chemical shift tensor. The chemical shift tensor results from a coupling of the electronic wavefunctions with the nuclei and, thus, mirrors changes in electronic structure brought about by chemical bonding.

(d) Motion of the protons can alter, or average, both the dipolar interactions responsible for the free induction decay lineshape and the chemical shift tensor and, in addition, can control the magnitude of a variety of relaxation times. The effect of motion on a variety of NMR relaxation times has been extensively reviewed with special emphasis on surface systems (3-8).

The use of conventional pulsed NMR techniques has been extensively discussed (22), and the comments here are limited to a discussion of the multiple pulse techniques and a discussion of the chemical shift tensor.

Multiple Pulse NMR Techniques. As the above discussion indicates, several

interactions contribute simultaneously to both the lineshape and associated relaxation effects of an NMR resonance. Although each of these interactions contains useful information, usually the NMR spectrum can be interpreted to give only the largest one or some complex combination of several. To allow further separation and characterization of the interactions present, a variety of recently developed multiple pulse NMR techniques may be used. These are, in general, characterized by the application of periodic and cyclic chains of intense rf pulses and have the effect of altering the effective size and character of specific interactions. Thus, use of these techniques can allow measurement of small interactions which are normally not measureable due to the presence of much larger interactions and can allow separation of interactions normally only measurable as a sum. Three such sequences were used in this work and are described below.

An eight-pulse cycle was used to remove the effects of static homonuclear dipolar broadening and to allow measurement of the proton chemical shift tensor. This pulse sequence has been discussed in detail previously (17,23), and it will only be pointed out here that it is essential to have the characteristic time associated with the pulse cycle shorter than the spin-spin relaxation time (the inverse of the dipolar linewidth), and that motional effects, particularly in the 10^{-4} to 10^{-6} sec. time domain, can interfere with the averaging process.

A phase altered version of the eight-pulse cycle (23, 24) was also used in this work. This sequence has the ability to remove the effect of static magnetic field inhomogeneities in addition to homonuclear dipolar interactions from the NMR spectrum. Thus, it can be used to determine what portion of the linewidth observed in the regular eight-pulse spectrum is due to magnetic

field inhomogeneities. As the chemical shift is, in effect, a magnetic field inhomogeneity, the phase altered eight-pulse cycle furnishes a means to be sure that the linewidth observed in the eight-pulse cycle can be attributed to chemical shift anisotropy and not to motional effects, experimental problems, or any residual homonuclear dipolar effects.

A Carr-Purcell sequence has been used here to separate the total dipolar interaction into contributions from homonuclear and heteronuclear interactions. The Meiboom-Gill (22) modification was used with the slight modification that two closely spaced 90^{o} pulses were used instead of a single 180^{o} pulse. By using previously described pulse adjustment procedures (16), very precise 180^{o} pulse rotations could be assured. The signal was sampled between each 180^{o} rotation.

Chemical Shift Tensor. The electron distribution surrounding a nucleus can distort the magnetic field at the nuclear site, and consequently, one observes a dependence of the resonance frequency on the nature of the chemical bonding present. As the electronic environment is normally not isotropic, this frequency dependence will show an angular dependence and is described by a chemical shift tensor. For the high field case this is a symmetric tensor and normally described by the three principal values of the tensor and the orientation of the principal axis coordinate system. The frequency shift induced by the chemical shift is normally not measurable in solids, but by using the multiple pulse NMR techniques to remove the dipolar broadening, it can be accurately determined. In single crystal samples one can determine both the principal values and the orientation of the principal axis system. However, in polycrystalline powders like the ones studied in this paper, one has present simultaneously many different orientations so that one observes a spectrum broadened by chemical shift effects. This "powder pattern" can be analyzed to extract the magnitude of the three principal values (25).

RESULTS AND DISCUSSION

100% Silica. The semilogarithmic plot of the free induction decay for the calcined sample of pure silica is shown in Figure 1. As is shown, the decay is exponential within the precision of the data. By extrapolating the line in Figure 1 back to zero time, an initial intensity is obtained which indicates 1.6 protons/100Å^2 ± 10% and a ratio of silicon atoms to protons of 11. The hydroxyl concentrations for silica samples treated at 500° C were found in the range 1.6 to 2.3 protons/100Å^2 by Davydov and coworkers (26), using chemical methods of analysis and a variety of preparation techniques. O'Reilly (9) found 2.6 protons/100Å^2, and more recently Freude (27) measured 0.87 protons/100Å^2, both using NMR techniques.

The time constant, T_2, for the free induction decay is 200 microseconds, and as an exponential decay in time space is equivalent to a Lorentzian line in frequency space, this is equivalent to a Lorentzian absorption spectrum with a full width at half height of 1600 Hz. A Lorentzian lineshape has been previously observed by O'Reilly and coworkers (5,9), who reported a T_2 of 180 microseconds which did not vary as a function of temperature between -210° and 280° C. Both the lack of a temperature dependence and results of the multiple pulse NMR measurements to be discussed below indicate that the Lorentzian lineshape is not the result of motional averaging. Lorentzian lineshapes have been predicted for a number of geometries where it is assumed that spins are distributed in a random fashion over only a small fraction of possible sites (28). It does not appear possible to use the results of such analytic treatments to extract any quantitative information on the distribution of hydroxyls on the silica. However, it is possible to draw the following quantitative conclusions: the hydroxyl groups are isolated,

that is, the protons do not exist in pairs (i.e., not as absorbed water), and the observed lineshapes are qualitatively consistent with the dilute spin model (27). These conclusions are in agreement with a number of infrared investigations which conclude that the remaining protons on silica surfaces after treatment at 500^{o} C are in isolated hydroxyl groups (1,2, 26,29).

The eight pulse cycle, with a cycle time of 96 microseconds, was applied to the calcined sample. As can be seen in Figure 2, the linewidth collapsed to near 250 Hz. One can conclude that the width and Lorentzian shape of the free induction decay were determined almost completely by dipolar interactions and furthermore that the dipolar interactions were essentially static on the timescale of 10^{-4} to 10^{-6} seconds. This furnishes evidence for the interpretation given above of the free induction decay lineshape.

The lineshape produced by the multiple pulse experiment has several potential sources: (1) inhomogeneous broadening, primarily chemical shift coupling, (2) time dependence, particularly in the dipolar interaction, and (3) residual instrumental broadening. The phase altered eight-pulse cycle was applied to further separate these effects as it will remove inhomogeneous broadening as well as static dipolar broadening. The line collapsed further to 32 Hz under the influence of the phase altered eight-pulse sequence, thus indicating that the lineshape in Figure 2 can be attributed to a chemical shift powder pattern broadened by bulk susceptibility effects. The smooth line through the data points in Figure 2 is a computer fit for an axially symmetric chemical shift tensor with a Lorentzian broadening function. The principal values furnished by the fit are $\sigma_{\perp}$ = -5.1 ppm and $\sigma_{\parallel}$ = +1.8 ppm relative to a spherical sample of tetramethylsilane (± 1 ppm). In order to correct

values for the effects of bulk susceptibility, the sample was approximated by an ellipsoid (a = b = 1/2 c, where a, b, and c are the semiaxes and with the magnetic field being along a), and the tabulated values of Osborn (30) were used with a value of -1.13×10^{-6} for the volume susceptibility to calculate a susceptibility correction of -1.4 ppm. Thus, susceptibility independent principal values for the hydroxyl protons on silica are $\sigma_{\perp} = -6.5$ ppm and $\sigma_{||} = +0.4$ ppm, and a susceptibility independent value for the trace, or isotropic portion, is -4.2 ppm (relative to TMS). A Lorentzian broadening function with a width of near 6 ppm was required to fit the spectrum in Figure 2, and this width is attributed primarily to smearing of the magnetic field at the surface of a particle whose magnetic susceptibility is different from the medium it is in.

A number of studies have recently been reported of the chemical shift tensor of both hydrogen bonded (31) and non-hydrogen bonded (32) hydroxyl protons, and all have reported tensors which exhibit an anisotropy ($\sigma_{||} - \sigma_{\perp}$) from 2 to 4 times the size of the 6.9 ppm found in this study. One can conclude either that the surface hydroxyl groups studied here have substantially altered chemical bonding from these solid state systems or that the value measured here has been partially averaged by an angular motion of the O--H vector (i.e., a wagging or rotation of the hydroxyl bond around the oxygen). Thus, while NMR data indicate that major motion, diffusion from oxygen site to oxygen site, does not occur, there is some indication that a local reorientation of the hydrogen around its oxygen may occur in this system. Hopefully, this point can be clarified by performing the multiple pulse measurements at low temperatures.

The same series of NMR measurements has been made on the rehydrated

sample of 100% silica with almost identical results. A surface concentration of 1.9 protons/100$\AA^2$ was determined from the free induction decay. This small increase of 0.3 protons/100$\AA^2$ suggests that the rehydration by water vapor is not reversible. Such irreversible rehydration has been reported earlier for silicas heat treated at temperatures over 400° C both by Young (33) and by Hockey and Pethica (34).

The lineshape for the rehydrated sample was Lorentzian within the precision of the data and indicates that the water molecules which were absorbed went on the surface as isolated hydroxyl groups. The principal values for the chemical shift tensor were determined as above and found to be $\sigma_{\perp}$ = -6.2 ppm and $\sigma_{\parallel}$ = +0.6 ppm, which are identical within experimental accuracy with the nonhydrated sample. Thus, essentially no difference between the two samples could be determined except for the small concentration difference noted above.

0% Silica (100% alumina). The logarithm of the amplitude of the free induction decay for the calcined alumina sample is shown versus time in Figure 3 and versus time squared in Figure 4. The proton concentration was 3.1 protons/100$\AA^2$, and the ratio of aluminum atoms to protons was 6.7. This higher concentration of protons on alumina compared to silica has been pointed out before (35). The linear plot in Figure 4 is the time response expected of a decay associated with a Gaussian lineshape, and from the slope of the line through the data points, one estimates a second moment of 2.8 gauss^2 for the proton line. This second moment has contributions from proton-proton interactions (homonuclear) and from proton-aluminum interactions (heteronuclear), and in order to separate these, a Carr-Purcell-Meiboom-Gill cycle was applied with a pulse spacing of 50 μ seconds. Assuming a Gaussian lineshape for the envelope of the echo maxima, an estimate of near 0.2 gauss^2

was obtained for the second moment. As the Carr-Purcell-Meiboom-Gill sequence removes static heteronuclear dipolar broadening as well as magnetic field inhomogeneity effects, the 0.2 gauss^2 can be attributed to homonuclear dipolar broadening (i.e., proton-proton broadening). This would imply that 2.6 gauss^2 of the proton second moment (i.e., essentially all of the 2.8 gauss^2 second moment measured) can be attributed to the heteronuclear (proton-aluminum) dipolar interaction. Also note that the small size of the proton-proton second moment implies widely separated protons on the alumina surface.

The rehydrated sample of alumina has a still higher concentration of hydroxyl groups, 4.4/100$\mathring{A}^2$, and was Gaussian within the experimental error, as is indicated in Figure 5. The second moment estimated from the slope of the line through the data points in Figure 5 is 3.7 gauss^2.

Silica-Aluminas. Compositions of 10, 25, 50, 75, and 90% silica were prepared, treated, and investigated as described above for the pure SiO_2 and Al_2O_3. Experimental results are presented in Figures 1, 3, 4, and 5 and in Table 1. A number of conclusions can be drawn from these results.

The 90 and 75% SiO_2 samples exhibited a single exponential decay for both calcined and rehydrated samples as can be seen in Figure 1. The concentrations of protons on these samples and estimates of the decay constants are given in Table 1. Using results and arguments from the discussion of the pure silica sample, the measured decay constants indicate that protons on these samples do not exist as closely spaced pairs (i.e., not as absorbed water) and do not exist in close proximity to an aluminum ion (i.e., not as AlOH groups). Again one notes that exponential decays, or Lorentzian lineshapes have been predicted for a number of geometries where it is assumed spins are distributed in a random fashion over only a small fraction of possible

sites (28). As in the case of pure silica, the eight-pulse sequence was applied to both the calcined and rehydrated 90% silica samples with results similar to those reported above for the pure silica, confirming that the observed decays were produced by static dipolar interactions.

The 50, 25, and 10% SiO_2 samples are quite different from the 75 and 90% samples. Figure 3 illustrates this point for the 50% SiO_2 calcined sample where a logarithmic plot is shown for the 100, 75, 50, and 0% calcined samples. The 50% SiO_2 decay consists of two components. At long times (>70 microseconds) it is qualitatively and quantitatively similar to the 75 and 100% SiO_2 decays, while at short times it is similar to the 0% (pure alumina) decay. In the analysis of the data of the pure alumina, the short decay was found to be due to the aluminum-proton dipolar interaction and was associated with hydroxyl groups attached to aluminum ions, while in the analysis of the 100, 90, and 75% SiO_2, the long decays were associated with isolated hydroxyls attached to silicon ions, i.e., SiOH groups. It is thus possible to separate quantitatively the fraction of protons bound to silicon and that fraction bound to aluminum. The intercept of the extrapolated line which fits the long-time behavior, as shown in Figure 3, is a measure of the SiOH density. The difference between this extrapolated intercept and the total intercept is a measure of the AlOH density on the sample. In order to compute this difference accurately, the 50% SiO_2 curve in Figure 4 was constructed by subtracting the amplitudes of the line extrapolated from the long-time portion shown in Figure 3 from the amplitudes of the data points in the short-time region. Thus, the 50% SiO_2 curve shown in Figure 4 represents the signal from the AlOH groups, and the intercept is directly proportional to the concentration of hydroxyl groups bound to aluminum ions.

The decays observed for the 50% SiO_2 rehydrated sample and both of the 25% SiO_2 samples also consisted of two components. Like the 50% SiO_2 calcined sample, the long-time portion was similar to the 100% SiO_2 decay, and the short-time portion was similar to the 100% Al_2O_3 decay. The number of hydroxyl groups bound to silicon ions and the number to aluminum ions were calculated in the same manner as above for the 50% SiO_2 calcined sample. For both 10% SiO_2 samples, the decays were similar to the 0% SiO_2 samples.

In order to compute second moments for the AlOH groups, a Gaussian decay was assumed. As can be seen from Figures 4 and 5, the straight lines, which are indicative of Gaussian behavior, fit the data for the 0 and 50% SiO_2 samples excellently, but fit the data for the 10 and 25% SiO_2 samples only moderately well. From the slopes of these lines, second moments were computed and are presented in Table 1. Almost all of the second moments for the AlOH groups were close to 2.8 $gauss^2$.

The entire results for the surface concentrations of AlOH groups and SiOH groups are presented in Table 1. It appears to be of substantial significance that AlOH groups were not detected on the 75% silica sample while nearly 75% of the protons on the 50% silica sample appear to be AlOH groups. Previous infrared work by Basila (36) has concluded that the existence of a single hydroxyl stretching frequency on a 75% silica implied only SiOH groups. Prior NMR work by O'Reilly, et al. (9) and Hall, et al. (10) on a 89% SiO_2 sample had limited the percent of surface protons in AlOH groups to less than 20%. The 75% silica sample contains one aluminum ion for every 2-1/2 silicon ions, but no measurable AlOH groups; the 50% silica contains one aluminum ion for each 0.85 silicon ion (54% aluminum ions), yet 75% of the hydroxyls are bound to the aluminum. These samples are all amorphous in the sense that no X-ray spectra are obtainable and infrared

data on Al-O and Si-O are broadened, yet the results presented here imply substantial order, specifically in the attachment of the hydroxyls.

There appears to be a clear qualitative change occurring in the nature of the hydroxyl groups between the 75 and 50% silica samples, with the 100, 90 and 75% being similar and exhibiting no detectable AlOH groups while the 50,25,10 and 0% SiO_2 have the bulk of their protons attached in close proximity to an aluminum ion. Further work on these samples involving infrared studies, surface titrations, and catalytic studies is in progress, and relationships between the NMR results and these studies will be published in the near future.

References

1. Hair, M. L., "Infrared Spectroscopy in Surface Chemistry," Marcel Dekker, New York, 1967.
2. Little, L. H., "Infrared Spectroscopy of Adsorbed Species," Academic Press, New York, 1966.
3. Aston, J. G., in "The Solid-Gas Interface " (E. A. Flood, Ed.), Vol. 2, p. 895. Marcel Dekker, New York, 1967.
4. Derouane, E. G., Fraissard, J., Fripiat, J. J., and Stone, W. E. E., Catal. Rev. 7, 121 (1972).
5. O'Reilly, D. E., in "Advances in Catalysis " (D. D. Eley, P. W. Selwood, and P. B. Weisz, Eds.), Vol. 12, p. 31. Academic Press, New York, 1960.
6. Packer, K. J., in "Progr. NMR Spectrosc." (J. M. Emsley, J. Feeney, and L. H. Sutcliffe, Eds.), Vol. 3, p. 81. Pergamon, London, 1968.
7. Pfeifer, H., in "NMR" (P. Diehl, E. Fluck, and R. Kosfeld, Eds.), Vol. 7, p. 53. Springer-Verlag, New York, 1972.
8. Resing, H. A., Advan. Mol. Relaxation Processes 1, 109 (1967-68).
9. O'Reilly, D. E., Leftin, H. P., and Hall, W. K., J. Chem. Phys. 29, 970 (1958).
10. Hall, W. K., Leftin, H. P., Cheselske, F. J., and O'Reilly, D. E., J. Catal. 2, 506 (1963).
11. Pearson, R. M., J. Catal. 23, 388 (1971).
12. Hall, W. K., private communication.
13. Schwarz, J. A., J. Vac. Sci. Technol., in press.
14. Kearby, K., Ph.D. Thesis, University of Illinois, 1937.
15. Schwarz, J. A., private communication.

16. Vaughan, R. W., Elleman, D. D., Stacey, L. M., Rhim, W.-K., and Lee, J. W., Rev. Sci. Instrum. 43, 1356 (1972).

17. Rhim, W.-K., Elleman, D. D., and Vaughan, R. W., J. Chem. Phys. 59, 3740 (1973).

18. Relcom, Mountain View, Calif.

19. Avantek, Inc., Santa Clara, Calif.

20. Abragam, A., "The Principles of Nuclear Magnetism," Oxford University Press, London, 1961.

21. Vaughan, R. W., in "Annual Reviews in Materials Science" (R. A. Huggins, R. H. Bube, and R. W. Roberts, Eds.), Vol. 4, p. 21. Annual Reviews, Palo Alto, 1974, and references therein.

22. Farrar, T. C., and Becker, E. D., "Pulse and Fourier Transform NMR," Academic Press, New York, 1971.

23. Rhim, W.-K., Elleman, D. D., Schreiber, L. B., and Vaughan, R. W., J. Chem. Phys. 60, 4595 (1974).

24. Dybowski, C. R., and Vaughan, R. W., Macromolecules 8, 50 (1975).

25. Bloembergen, N., and Rowland, T. J., Phys. Rev. 97, 1679 (1955).

26. Davydov, V. Ya., Zhuravlev, L. T., and Kiselev, A. V., Trans. Faraday Soc. 60, 2254 (1964).

27. Freude, D., Müller, D., and Schmiedel, H., Surface Sci. 25, 289 (1971).

28. Rakvin, B., and Herak, J. N., J. Magn. Resonance 13, 94 (1974) and references therein.

29. McDonald, R. S., J. Phys. Chem. 62, 1168 (1958).

30. Osborn, J. A., Phys. Rev. 67, 351 (1945).

31. Haeberlen, U., Proceedings of the 1st Specialized Colloque Ampère, Krakow, Poland, p. 28 (1973);

Vaughan, R. W., Rhim, W.-K., and Elleman, D. D., Proceedings of the 1st Specialized Colloque Ampère, Krakow, Poland, p. 129 (1973);
Haubenreisser, U., and Schnabel, B., Proceedings of the 1st Specialized Colloque Ampère, Krakow, Poland, p. 140 (1973);
Van Hecke, P., Weaver, J. C., Neff, B. L., and Waugh, J. S., Proceedings of the 1st Specialized Colloque Ampère, Krakow, Poland p. 143 (1973);
J. Chem. Phys. 60, 1668 (1974);
Haeberlen, U., and Kohlschütter, U., Chem. Phys. 2, 76 (1973);
Raber, H., Brunger, G., and Mehring, M., Chem. Phys. Letters 23, 400 (1973);
Haeberlen, U., Kohlschütter, U., Kempt, J., Spiess, H. W., and Zimmermann, H., Chem. Phys. 3, 248 (1974);
Willsch, R., Burghoff, U., Müller, R., Rosenberger, H., Scheler, G., Pettig, M., and Schnabel, B., Proceedings of the 18th Ampère Congress, Nottingham, p. 553, 1974.

32. Schreiber, L. B., and Vaughan, R. W., Chem. Phys. Letters 28, 586 (1974).
33. Young, G. J., J. Colloid Sci. 13, 67 (1958).
34. Hockey, J. A., and Pethica, B. A., Trans. Faraday Soc. 57, 2247 (1961).
35. Haldeman, R. G., and Emmett, P. H., J. Amer. Chem. Soc. 78, 2917 (1956).
36. Basila, M. R., J. Phys. Chem. 66, 2223 (1962).

Table 1

Summary of proton NMR results for calcined and rehydrated silica-aluminas of varying composition.

Weight % SiO_2	Surface Area m^2/gm	Calcined Samples				Rehydrated Samples			
		SiOH		AlOH		SiOH		AlOH	
		σ_2 #H/100A^2	T_2 µsec	σ_2 #H/100A^2	$M_2{}^2$ gauss^2	σ_2 #H/100A^2	T_2 µsec	σ_2 #H/100A^2	$M_2{}^2$ gauss^2
100	576	1.6	200	---	---	1.9	170	---	---
90	693	1.5	160	---	---	3.2	120	---	---
75	615	1.2	150	---	---	1.8	140	---	---
50	727	1.0	140	2.7	2.7	1.0	105	3.5	2.9
25	839	0.2	160	2.4	2.7	.5	80	3.7	2.9
10	768	---	---	3.4	2.7	---	---	4.4	3.0
0	571	---	---	3.1	2.8	---	---	4.4	3.7

Figure Captions

Figure 1: Plot of free induction decay envelope vs. time for samples of varying SiO_2 composition. Data from the various samples have been displaced vertically in order to clarify presentation. The values of T_2 reported in Table 1 were obtained from the slopes of the lines placed through the data.

Figure 2: Powder pattern using eight-pulse cycle of 100% SiO_2 calcined sample. The signal amplitude is plotted vs. chemical shift (ppm) relative to TMS.

Figure 3: Plot of free induction decay envelope vs. time for calcined samples of varying SiO_2 composition. Data from the various samples have been displaced vertically in order to clarify presentation.

Figure 4: Plot of decay envelope of AlOH groups vs. time squared for calcined samples of varying SiO_2 composition. Data from the various samples have been displaced vertically in order to clarify presentation. The values of second moment reported in Table 1 were obtained from the slopes of the lines placed through the data.

Figure 5: Plot of decay envelope of AlOH groups vs. time squared for rehydrated samples of varying SiO_2 composition. Data from the various samples have been displaced vertically in order to clarify presentation. The values of second moment reported in Table 1 were obtained from the slopes of the lines placed through the data.

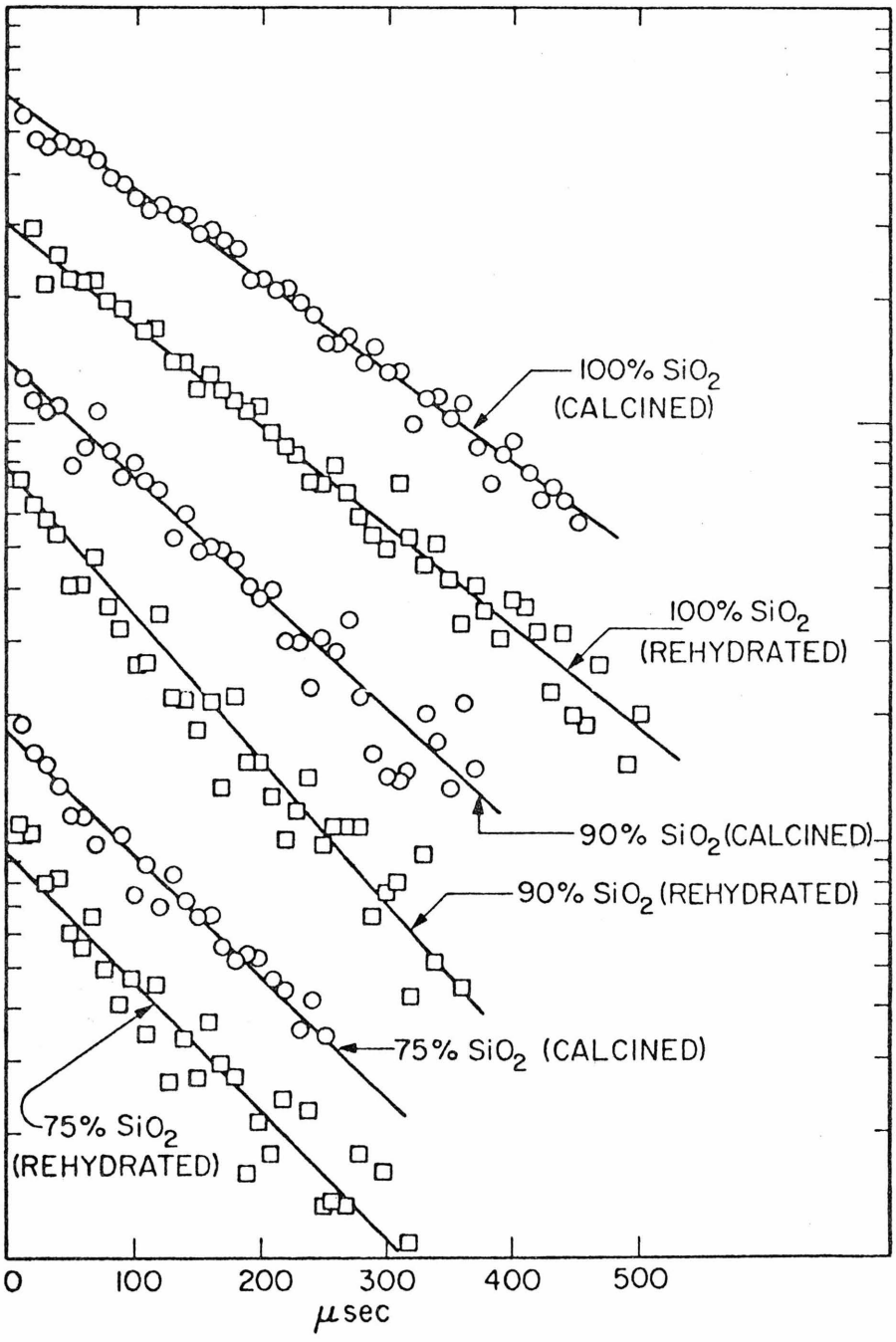
100% SiO2
(CALCINED)
100% SiO2
(REHYDRATED)
90% SiO2 (CALCINED)
90% SiO2 (REHYDRATED)
75% SiO2 (CALCINED)
75% SiO2
(REHYDRATED)
0
100
200
300
400
500
μsec

Fig.1

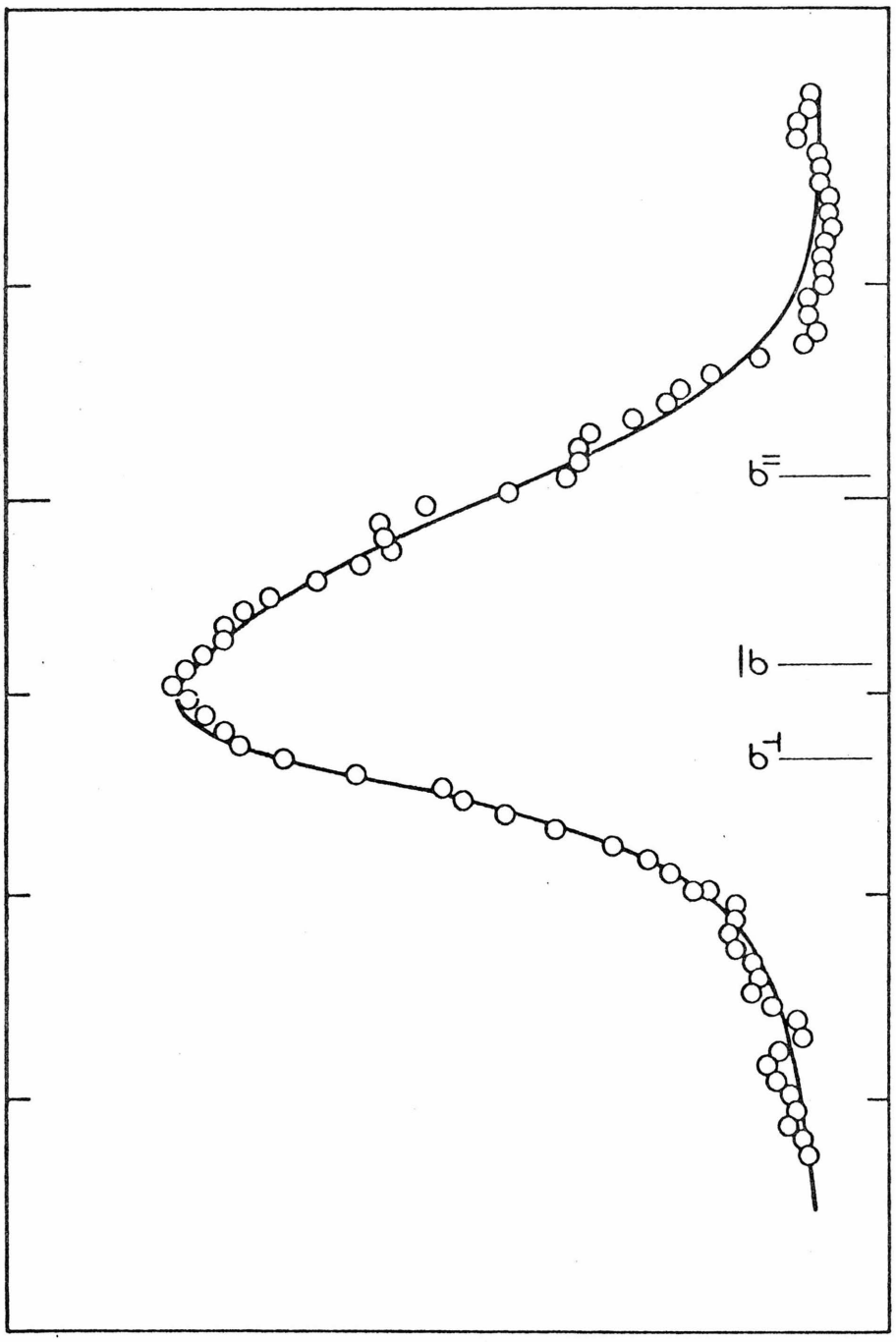

Fig.2

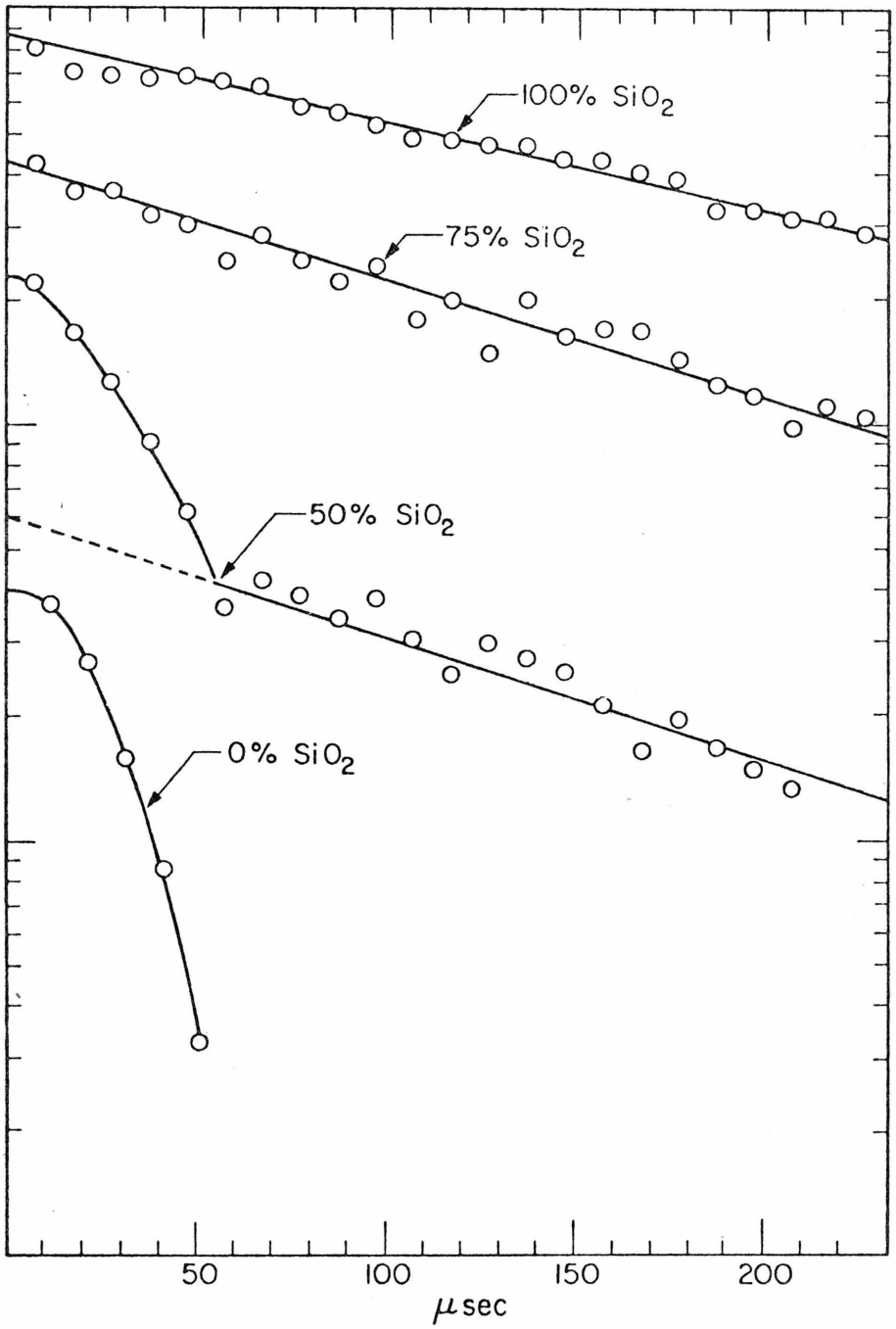

Fig.3

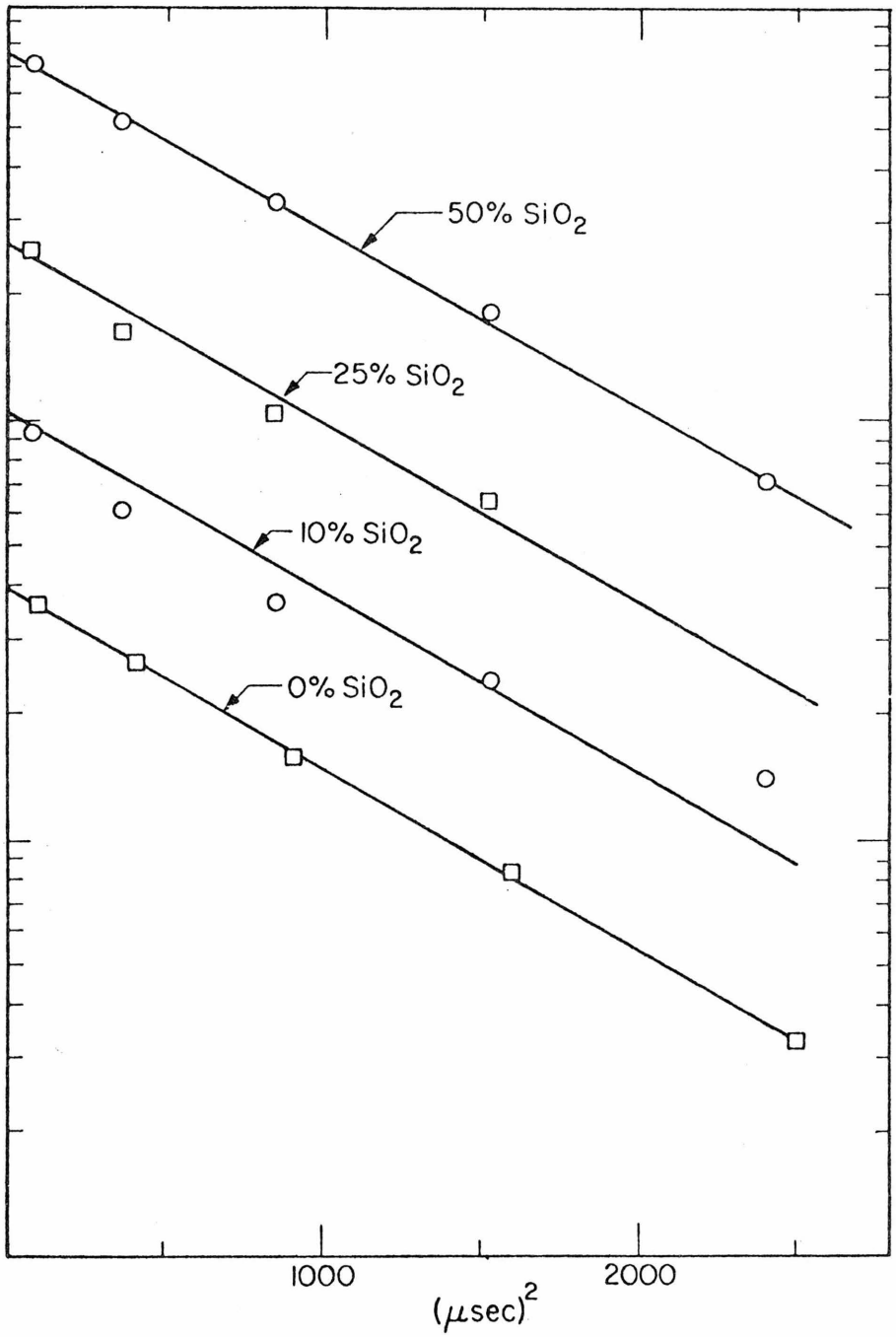

Fig.4

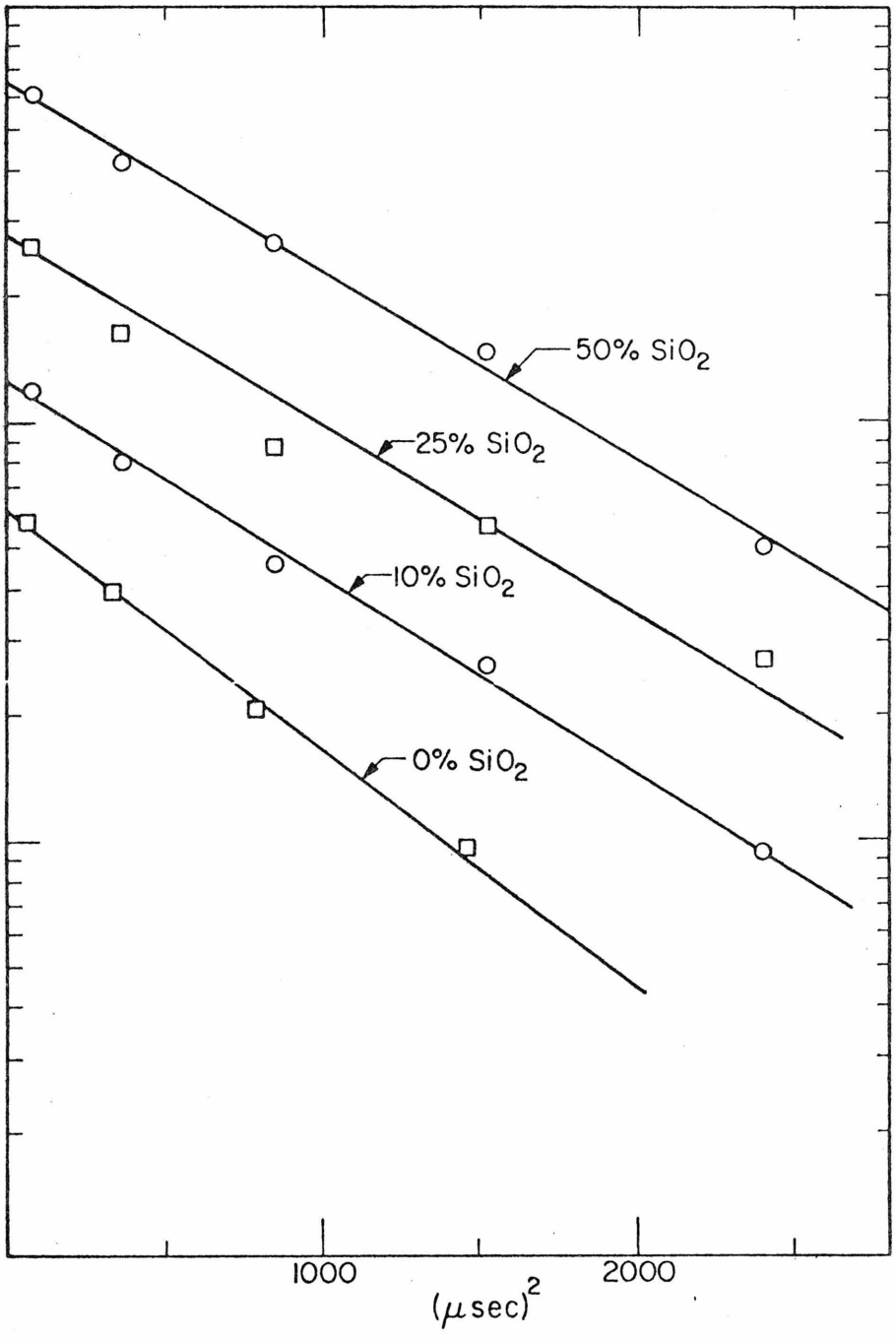

Fig.5

CHAPTER 5

CONCLUSIONS

The analysis, which is presented in Chapter 2, shows that the effects of pulse errors on multiple pulse spectra may be easily calculated by extending the Average Hamiltonian formalism. The method described in Chapter 2 offers distinct advantages over previous treatments because (i) a large class of pulse imperfections can be examined directly, (ii) the analytical form allows pulse cycle imperfections to be treated in a general fashion, and (iii) it is possible to use the formulation of the Average Hamiltonian treatment to sort out and understand the detailed physics of the interactions of pulse trains which have several types of imperfections present simultaneously.

Application of the theoretical analysis of Chapter 2 has shown the following:

(1) A simple geometric picture described the effects of the average pulse-imperfection Hamiltonians upon the time development of the magnetization. Furthermore, this geometric picture also shows how the effects of pulse errors upon second averaging may be calculated.

(2) Rational procedures can be formulated for systematically tuning the spectrometer to eliminate phase errors, pulse length errors, and phase transient errors. These procedures are applicable to most common pulse cycles.

(3) The eight-pulse cycle is superior to the four-pulse cycle for narrowing dipolar-broadened lines in solids. For the eight-pulse cycle, phase errors, phase transients, pulse length errors, H_1 inhomogeneity, and the finite width of pulses do not diminish resolution to first order. Thus, the eight-pulse cycle provides good resolution, is easy to tune-up, and remains exceptionally stable. In order to do high

resolution NMR on solids, one does not need to build a perfect spectrometer, just a good one.

The principal values of the proton chemical shift tensor of $Ca(OH)_2$ are $\sigma_{\perp}$ = -9.3 ± 1 ppm and $\sigma_{||}$ = +4.7 ± 1 ppm relative to TMS. This chemical shift tensor is the only one that has been reported for non-hydrogen-bonded hydroxyl groups. The proton chemical shift anisotropy for $Ca(OH)_2$, which is 14 ± 1 ppm, is substantially smaller than proton chemical shift anisotropies for hydrogen bonded protons, which are in the range 18 to 26 ppm.

In addition to providing experimental results for comparison with theoretical calculations, measurements of the chemical shift tensor on well-defined single crystals also help empirically to interpret data and to characterize protons in complicated systems such as adsorbed molecules on a surface.

A combination of conventional and multiple pulse NMR techniques has been used to examine the hydroxyl protons on a series of high surface area silica-aluminas whose composition varied from 0-100% SiO_2. Multiple pulse NMR can be effectively used to sort out possible spin-lattice interactions in this complicated adsorption system. In particular, the eight-pulse cycle can be used to prove the presence of a static proton-proton dipolar coupling while the Meiboom-Gill cycle can be used to prove the presence of a static proton-aluminum coupling.

Both calcined and rehydrated silica-aluminas have the following

characteristics:

(1) Protons are immobile on the timescale of 10^{-6} to 10^{-5} seconds.

(2) Hydroxyl groups are isolated.

(3) No AlOH groups are detectable on high silica content surfaces, 75-100% SiO_2.

(4) Most protons are in AlOH groups on 50% and lower SiO_2 content surfaces.

(5) The chemical shift tensor of protons on a pure SiO_2 surface is axially symmetric and the chemical shift anisotropy is +6.9 ± 1 ppm.

Characteristics 3 and 4 above suggest a major change in local structure between 75% and 50% silica content.

This thesis has described new theoretical and experimental developments in multiple pulse NMR. These developments allow multiple pulse NMR to be used with confidence under adverse conditions such as low signal-to-noise ratios and strong dipolar couplings. Multiple pulse NMR has been used for the first time to help to characterize a chemisorbed system. Results of this initial study on silica-aluminas are promising. Additional NMR studies on silica-aluminas and other oxide surfaces should be encouraged.